

1 Intra- and inter-annual changes in isoprene emission from central Amazonia

2
 3 Eliane Gomes Alves^{1,2*}, Raoni Aquino Santana³, Cléo Quaresma Dias-Junior^{4,2}, Santiago
 4 Botía⁵, Tyeen Taylor⁶, Ana Maria Yáñez-Serrano^{7,8,9}, Jürgen Kesselmeier¹⁰, Efstratios
 5 Bourtsoukidis¹¹, Jonathan Williams¹², Pedro Ivo Lembo Silveira de Assis¹³, Giordane
 6 Martins¹³, Rodrigo de Souza¹⁴, Sergio Duvoisin Junior¹⁵, Alex Guenther¹⁶, Dasa Gu¹⁷,
 7 Anywhere Tsokankunku¹², Matthias Sörgel¹², Bruce Nelson¹⁸, Davieliton Pinto¹³, Shujiro
 8 Komiya¹, Diogo Martins Rosa¹³, Bettina Weber^{19,10}, Cybelli Barbosa^{10,19}, Michelle Robin¹,
 9 Kenneth J Feeley²⁰, Alvaro Duque²¹, Viviana Londoño Lemos²², Maria Paula Contreras²³,
 10 Alvaro Idarraga²⁴, Norberto López A.²⁴, Chad Husby²⁵, Brett Jestrow²⁵, Iván Mauricio
 11 Cely Toro⁴.

12
 13 ¹ Department of Biogeochemical Processes, Max Planck Institute for Biogeochemistry, Jena, Germany

14 ² Climate and Environment Department, National Institute of Amazonian Research, Manaus, Brazil

15 ³ Department of Atmospheric Sciences, Federal University of Western Para, Santarem, Brazil

16 ⁴ Federal Institute of Para, Belem, Brazil

17 ⁵ Department of Biogeochemical Signals, Max Planck Institute for Biogeochemistry, Jena, Germany

18 ⁶ Department of Civil & Environmental Engineering, University of Michigan, USA.

19 ⁷ IDAEA-CSIC, 08034, Barcelona, Spain

20 ⁸ CREAM, E08193 Bellaterra (Cerdanyola del Vallès), Catalonia, Spain

21 ⁹ Global Ecology Unit, CREAM-CSIC-UAB, E08193 Bellaterra (Cerdanyola del Vallès), Catalonia, Spain

22 ¹⁰ Multiphase Chemistry Department, Max Planck Institute for Chemistry, Mainz, Germany

23 ¹¹ The Cyprus Institute, Nicosia, Cyprus

24 ¹² Atmospheric Chemistry Department, Max Planck Institute for Chemistry, Mainz, Germany

25 ¹³ Department of Tropical Forest Sciences, National Institute for Amazonian Research, Manaus, Brazil

26 ¹⁴ Meteorology Department, State University of Amazonas, Manaus, Brazil

27 ¹⁵ Chemistry Department, State University of Amazonas, Manaus, Brazil

28 ¹⁶ Department of Earth System Science, University of California, Irvine, U.S.A.

29 ¹⁷ Division of Environment and Sustainability, Hong Kong University of Science and Technology, Clear
 30 Water Bay, Hong Kong, China

31 ¹⁸ Coordination of Environmental Dynamics, National Institute of Amazonian Research, Manaus, Brazil

32 ¹⁹ Institute for Biology, Division of Plant Sciences, University of Graz, Graz, Austria

33 ²⁰ Department of Biological Sciences, University of Miami, Coral Gables, FL, USA.

34 ²¹ Departamento de Ciencias Forestales, Universidad Nacional de Colombia–Sede 19 Medellín, Medellín,
 35 Colombia

36 ²² Department of Plant and Microbial Biology, University of Minnesota, USA

37 ²³ Jardín Botánico de Cartagena “Guillermo Piñeres”, Turbaco, Bolívar, Colombia.

38 ²⁴ Fundación Jardín Botánico de Medellín, Antioquia, Colombia.

39 ²⁵ Fairchild Tropical Botanic Garden, Miami, FL, USA

40 *egomes@bgc-jena.mpg.de

42 Abstract

43 Isoprene emissions are a key component in biosphere-atmosphere interactions, and the
 44 most significant global source is the Amazon rainforest. However, intra- and inter-annual
 45 variations in biological and environmental factors that regulate isoprene emission from
 46 Amazonia are not well understood and, thereby, poorly represented in models. Here, with
 47 datasets covering several years of measurements at the Amazon Tall Tower Observatory
 48 (ATTO), in central Amazonia, Brazil, we (1) quantified canopy profiles of isoprene mixing
 49 ratios across seasons of normal and anomalous years and related them to the main drivers

50 of isoprene emission – solar radiation, temperature, and leaf phenology; (2) evaluated the
51 effect of leaf age on the magnitude of the isoprene emission factor (E_s) from different tree
52 species and scaled up to canopy with intra- and inter-annual leaf age distribution derived
53 by a phenocam; and (3) adapted the leaf age algorithm from MEGAN with observed
54 changes in E_s across leaf ages. Our results showed that the variability in isoprene mixing
55 ratios was higher between seasons (max. during the dry-to-wet transition seasons) than
56 between years, with values from the extreme 2015 El-niño year not significantly higher
57 than in normal years. In addition, model runs considering in-situ observations of canopy E_s
58 and the modification on the leaf age algorithm with leaf-level observations of E_s presented
59 considerable improvements in the simulated isoprene flux. This shows that MEGAN
60 estimates of isoprene emission can be improved when biological processes are
61 mechanistically incorporated into the model.

62

63

63 1. Introduction

64

65 Isoprene dominates the emission of biogenic volatile organic compounds (BVOCs) into
66 the atmosphere, and its major global source is tropical vegetation (Guenther et al., 2012;
67 Sindelarova et al., 2014). In the atmosphere, isoprene is a short-lived (minutes to hours)
68 reactive BVOC species, and its photooxidation affects the atmospheric oxidation capacity
69 contributing to the formation of ozone (O_3) and secondary organic aerosols (SOA)
70 (Atkinson, 1997; Pöschl et al., 2010). With its high plant foliage biomass and rich plant
71 diversity (ter Steege et al., 2013), the Amazon Forest represents a key source of isoprene
72 to the atmosphere (Yáñez-Serrano et al., 2020). However, model estimates of isoprene
73 emission and its intra- and inter-annual variability in the Amazon still carry high
74 uncertainty, because only a few observational experiments have been conducted with
75 mechanistic and process-based approaches, which hinders further modeling optimization
76 (Alves et al., 2018; Yáñez-Serrano et al., 2020). One of the most critical knowledge gaps
77 is how plants' isoprene emission differs under extremely hot and dry conditions, such as in
78 El-niño years, and how this might affect atmospheric processes. As some studies have
79 indicated that extreme years will become more frequent and intense with climate change
80 (Nobre et al., 2016; Boulton et al., 2022), it is essential to understand the processes
81 mediated by isoprene in such years to improve model estimates (Yáñez-Serrano et al.,
82 2020; Artaxo et al., 2022).

83

84 Some reasons for uncertainties in isoprene model estimates are already known. The correct
85 determination of the magnitude of the isoprene source - or the emission factor at leaf
86 standard conditions ($1000 \mu\text{mol m}^{-2} \text{s}^{-1}$ photosynthetically active radiation- PAR, $30 \text{ }^\circ\text{C}$),
87 as it is conceptualized in models (e.g., Guenther et al., 1995) - is crucial to improve isoprene
88 modeling estimates. The Amazon plant biodiversity represents a considerable challenge for
89 determining the isoprene emission factor. Although previous studies suggested that $\sim 1\%$
90 of tree species are hyperdominant - with their tree individuals responsible for half of all
91 tree stems, carbon storage, and productivity (ter Steege et al., 2013; Fauset et al., 2015) -,
92 it is still unclear which plant species can emit substantial amounts of isoprene (Monson et
93 al., 2013), how these isoprene emitters are distributed throughout the Amazon basin, and
94 how the isoprene emission factor varies seasonally and interannually as result of changes
95 in eco-physiological processes (Gomes Alves et al., 2022). Another source of uncertainty

96 is related to quantifying the main sinks of isoprene. Once emitted by plant foliage, isoprene
97 can undergo surface deposition onto plant canopy (Karl et al., 2004) and soil (Pegoraro et
98 al., 2006), can be oxidized at rates depending on the atmospheric concentration of other
99 gases such as NO_x, O₃ and OH (Atkinson, 1997), and can be transported into and out of the
100 atmospheric boundary layer (Wei et al., 2018). Additionally, the rapid conversion of
101 isoprene photooxidation products can open a further sink for BVOCs in plants. This
102 chemical and biological processing of emitted compounds may affect vertical transport
103 processes, again influencing the biosphere (Kesselmeier et al., 2002; Canaval et al., 2020).
104

105 In addition, seasonal variation in isoprene emission from Amazon forests has been reported
106 by several in-situ studies, with the indication that isoprene seasonality is driven by intra-
107 annual variation in solar radiation, temperature, and leaf phenology (Kuhn et al., 2004a, b;
108 Yáñez-Serrano et al., 2015; Alves et al., 2016, 2018; Wei et al., 2018; Langford et al.,
109 2022). On a larger scale, satellite retrievals of isoprene oxidation products, like
110 formaldehyde (Barkley et al., 2009; Bauwens et al., 2016), and direct retrieval of isoprene
111 (Fu et al., 2019; Wells et al., 2022) have given an initial view of the long-term Amazon
112 isoprene emission, enabling not only seasonal but also inter-annual comparisons. Yet, there
113 remains a need to parameterize and evaluate the estimations with local and regional
114 measurements and to gain a better understanding of the main processes related to sources
115 and sinks of isoprene, since some studies have shown that satellite-derived isoprene
116 emission values are either overestimated (Alves et al., 2016) or underestimated (Gu et al.,
117 2017), or even show maximum emissions in a different season when compared to in-situ
118 measurements (Alves et al., 2016, 2018).
119

120 Here we report in-situ observations of isoprene mixing ratios during different seasons and
121 in consecutive years in central Amazonia to evaluate intra- and inter-annual variabilities in
122 two normal years (2013-2014) and one El-niño year (2015); in addition, we report
123 observations of leaf-level isoprene emission factor and leaf phenology monitoring. With
124 the intra- and inter-annual observations of isoprene at a central Amazonian site, this study
125 proposes to: (1) quantify the isoprene mixing ratios across seasons of normal and
126 anomalous years and compare them with the main drivers of isoprene emission – solar
127 radiation, temperature, and leaf phenology; (2) evaluate the effect of leaf age on the
128 magnitude of the isoprene emission factor from different tree species and scale up with
129 canopy intra- and inter-annual leaf age distribution; and (3) use the Model of Emissions of
130 Gases and Aerosols from Nature (MEGAN) to assess the effects of the observed changes
131 in the isoprene emission factor across leaf ages, by modifying the leaf age algorithm and
132 comparing simulations with observations at canopy-level.
133

134

135

2. Methods

136 2.1 Amazon Tall Tower Observatory (ATTO)

137

138 We performed measurements at the ATTO site located 150 km northeast of Manaus in the
139 Uatumã Sustainable Development Reserve (USDR) in central Amazonia. The climate is
140 tropical humid, with two distinctive seasons – wet season (December-May) and dry season

141 (July-October) and transition seasons in between – and has a mean annual precipitation of
142 2380 mm (TRMM climatological average – 1998-2019; please see more details in Botía et
143 al., 2022). The vegetation in this area is considered mature, mostly non-flooded rainforest
144 (terra-firme), with a mean canopy height of 35 m, and predominantly occurs on plateaus at
145 a maximum altitude of approximately 130 m a.s.l. (Andreae et al., 2015). Air masses
146 arriving at the site predominantly come from the east (NE~20%, ENE~27%, E~33%,
147 ESE~19%) (Zannoni et al., 2020) and have passed through 1500 km of undisturbed terra-
148 firme rainforest, with minor intrusion of air masses from Manaus (Pöhlker et al.,
149 2019). Figure 1 shows seasonal variation in solar radiation, air temperature, precipitation,
150 and soil moisture from 2013 to 2019. Andreae et al. (2015) have more details on this
151 experimental site.

152

153 *2.2 Mixing ratios of isoprene – canopy level*

154

155 Isoprene gradient mixing ratios were inferred by air samples collected from the INSTANT
156 tower (80 m height, coordinates: S 02°08.7520' W 58°59.9920') at eight heights in and
157 above the canopy (0.05, 0.5, 4, 12, 24, 38, 53 and 79 m) during intensive campaigns across
158 different seasons from November 2012 to October 2015. Eight heated (50 C) and insulated
159 inlets (fluorinated ethylene propylene - FEP, OD $\frac{3}{8}$ in.) were connected to a quadrupole
160 Proton Transfer Reaction – Mass Spectrometer (PTRMS) (Ionicon Analytic GmbH,
161 Austria) - using the primary ion H₃O⁺ and operated under standard conditions (2.2 mbar
162 drift pressure, 600V drift voltage, 127 Td), which was housed in an air-conditioned
163 container 10 m from the INSTANT tower. The inlets were guided to a valve system,
164 switching every 2 min between the different heights, completing a full profile in 16 min.
165 While an inlet was not sampled, it was flushed by a bypass pump at a flow rate of 16 lpm.
166 Humidity-dependent calibrations (using bubbled synthetic zero air to dilute the standard,
167 regulated as close as possible to ambient humidity conditions) were performed using a gas
168 cylinder containing isoprene (m/z 69). The dilution steps ranged from 22 to 0.8 ppb. To
169 determine the background signal for isoprene, a catalytic converter (Supelco, Inc. with
170 platinum pellets heated to >400 °C) was used to convert ambient VOC to CO₂ +H₂O. The
171 background signal was measured once every hour and then interpolated over the time of
172 the measurements. The detection limit (LOD) for isoprene varied between 0.09 (wet
173 season) and 0.1 (dry season) ppb. The mean total uncertainty of isoprene mixing ratios was
174 9.9 %, within the PTRMS measurement uncertainty (~10%). For more details on the
175 experimental setup, PTRMS conditions, and calibration, we refer the reader to Yáñez-
176 Serrano et al. (2015)

177

178

179 *2.3 Flux of isoprene – canopy level*

180

181 During a campaign in November 2015, eddy covariance fluxes of isoprene were measured
182 for 11 days. Isoprene concentrations were obtained with the above-described PTRMS at a
183 time resolution of 1 s and from a separate $\frac{3}{8}$ " inlet at 41 m height that sampled air at a
184 flow rate of about 10 l min⁻¹. A CSAT3 sonic anemometer (Campbell Scientific Inc.,
185 Logan, U.S.A.) measured the three-dimensional wind speed at high frequency (1 Hz) and
186 was placed at a distance of 0.5 m from the isoprene inlet. Fluxes were then calculated by

187 correlating fluctuations of the vertical wind vector to the fluctuations of isoprene
188 concentrations with the software package EddyPro® (LI-COR Inc., Lincoln, U.S.A.). A
189 method for despiking and raw data statistical screening was employed (Vickers and Mahrt,
190 1997). Half-hourly averaged fluxes were flagged according to a method of data quality
191 control (Mauder and Foken, 2004), and only data with the highest quality (flags 0 and 1)
192 was used for further analyses. Losses for sampling frequencies between 0.1 and 0.8Hz have
193 been observed as below 10% (Guenther and Hills, 1998; Spirig et al., 2005; Holst et al.,
194 2010; Jensen et al., 2018). Footprints were calculated using a two-dimensional model for
195 a geographic domain of 2 x 2 km centered at the INSTANT tower (Kljun et al., 2015). The
196 Tovi Footprint Analysis Toolbox (LI-COR Inc., Lincoln, U.S.A.) was used to calculate
197 half-hourly footprints and to combine them for the measurement period. Mean daytime
198 uncertainties of eddy covariance isoprene flux were at most 15%. More details on the flux
199 measurements and data processing are given in Pfannerstill et al. (2018).

200

201 *2.4 Leaf Area Density – measurements with the Light Detection and Ranging sensor* 202 *(LiDAR)*

203

204 Measurements of canopy leaf area density were carried out with a ground Light Detection
205 and Ranging sensor (LiDAR) at the ATTO site. These measurements aimed to give
206 information on the canopy structure around the INSTANT tower. Ground-LiDAR surveys
207 were conducted in October 2015 with a Riegl LD90-3100VHS-FLP system (Horn,
208 Austria), which generated a canopy profile map in vertical and horizontal directions. We
209 walked ten transects of 150 m in length with the ground-LiDAR system. The transects were
210 parallelly distributed at a distance of ~ 100 m from each other, with six transects to the
211 east/northeast, three transects to the west, and one transect to the south of the INSTANT
212 tower. Measurements were averaged every 15 m of each transect, summing up to ten
213 measurements per transect. Measurements of all ten transects were then averaged and
214 presented with the confidence interval (95%). More details about how the ground LiDAR
215 data were analyzed can be obtained from Stark et al. (2012).

216

217 *2.5 Leaf-level monitoring of leaf demography and phenology*

218

219 Leaf demography and phenology of 36 trees were monitored from March 2016 to
220 December 2017. Along 100 m of canopy walkways, canopy leaves were monitored
221 monthly to determine leaf ages and investigate how leaf age proportions vary during the
222 year. Ten branches of each tree were randomly selected and labeled with one iron ring at
223 their bottom end. All leaves attached from the bottom to the apical end were counted and
224 dated according to the day of observation. For the first observation, all leaves were assigned
225 with unknown age. In the following months, every time a new leaf was observed, the date
226 of observation was recorded for that specific leaf. For leaf age determination, the date of
227 the first observation of a new leaf was set back to 15 days before observation. The age was
228 calculated by the difference, in the number of days, between the first day and the last day
229 of observation, resulting in a number of days with a deviation of plus-minus 15 days. For
230 instance, if a new leaf was observed on 1st July 2017, the flushing date of this leaf was
231 assigned for 17th June 2017 (+/- 15 days). Then, all subsequent measurements considered

232 17th June 2017 as a date for leaf flushing, and aging was counted based on the number of
 233 days that this leaf stayed attached to the branch.

234

235 *2.6 Isoprene emission factor – leaf level*

236

237 Leaves of 21 canopy tree species, out of the 36 trees monitored for leaf demography and
 238 phenology (described in section 2.5), were measured to determine the isoprene emission
 239 factor across different leaf ages (Table S1) from October to November 2017. The other 15
 240 trees were unreachable with the sampling system and, therefore, not measured. Leaf-level
 241 isoprene sampling was carried out in 2-3 leaves of each age class available for each tree
 242 during the measurement period, using a commercial portable gas exchange system GFS-
 243 3000 (Walz, Effelthich, Germany). Each leaf was separately enclosed in the leaf chamber
 244 at standard conditions – photosynthetic photon flux density (PPFD) set to 1000 $\mu\text{mol m}^{-2}$
 245 s^{-1} and leaf temperature to 30°C - until net assimilation, stomatal conductance and internal
 246 CO_2 concentration were stable. The measurement stability criterion was assigned as one
 247 standard deviation of the net assimilation mean. The airflow rate going into the leaf
 248 chamber was 400 $\mu\text{mol s}^{-1}$ and CO_2 and H_2O concentrations were 400 $\mu\text{mol.mol}^{-1}$ and 21
 249 mmol.mol^{-1} (relative humidity of ~60%), respectively. Air exiting the GFS-3000 leaf
 250 chamber was routed to fill sorbent cartridges (stainless steel tubes filled with Tenax TA
 251 and Carbograph 5 TD sorbents), and a downstream pump sampled the exiting air at a rate
 252 of 200 sccm for 10 min. A hydrocarbon filter (Restek Pure Chromatography, Restek
 253 Corporations, USA) was installed at the air inlet of GFS-3000 to remove isoprene from the
 254 incoming ambient air, and all tubing in contact with the sampling air was made of PTFE.
 255 Before each measurement, a blank sample was obtained from the empty leaf chamber.

256

257 Isoprene content in the sorbent cartridges was determined in the laboratory at the
 258 University of California (Irvine, U.S.A.). All cartridges were placed into a thermally
 259 desorbing autosampler (TD-100, Markes International, Inc). The isoprene was pre-
 260 concentrated at 10 °C followed by injection into a gas chromatograph (GC, model 7890B,
 261 Agilent Technologies, Inc) equipped with a time-of-flight mass spectrometer (Markes
 262 BenchTOF-SeV) and a flame ionization detector (TD-GC-FID/TOF-MS) (Woolfenden
 263 and McClenny, 1999; ASTM D6196-15, 2015). Internal standards tetramethylethylene
 264 and decahydronaphtalene were injected into each sample after collection and before
 265 analysis. The system was calibrated daily with a commercial isoprene standard from Apel
 266 Riemer Environmental Inc. The external gas standard was prepared using a dynamic
 267 dilution system, and the effluent was added to sorbent cartridges under conditions similar
 268 to those used for sampling. Once the volume mixing ratio of isoprene (ppbv) was obtained,
 269 leaf emission flux was determined using the Eq. (1):

270

271

$$F = R_{ppbv} \times \frac{Q}{A} \quad (1)$$

272

273 where F ($\text{nmol.m}^{-2}.\text{s}^{-1}$) is leaf flux of isoprene emission; R_{ppbv} (nmol.mol^{-1}) is isoprene
 274 concentration of the sample (cartridge); Q is the flow rate of air into the leaf chamber (400
 275 $\mu\text{mol.s}^{-1}$); and A is the area of leaf within the chamber (0.08 m^2). The isoprene emission
 276 rate was then calculated and converted to $\text{mg.m}^{-2}.\text{h}^{-1}$. For more details on tree species, leaf
 277 age, and assigned leaf age class, see Table S1 in Supplementary Information.

324 2.7 Tower-camera derived leaf phenology and demography data

325

326 Upper canopy leaf phenology was monitored with a Stardot RGB camera (model Netcam
327 XL 3MP) installed at 81m height on the ATTO INSTANT tower. For more details on the
328 camera setup, radiometric calibration, and detection of phenological stages, we refer the
329 reader to Lopes et al. (2016). Only images acquired near noon and under an overcast sky
330 (diffuse illumination) were selected for subsequent analysis. The camera (subsequently
331 called phenocam) monitored the upper crown surfaces of 194 trees from July 2013 to
332 November 2018. Images were analyzed to track the temporal trajectory of each tree crown
333 and assign them into one of three classes: “leaf flushing” (crowns that showed a strong
334 increase in greening), “leaf abscising” (crowns which showed a large increase in greying,
335 which is the color of bare upper canopy branches) or “no change”. By counting the number
336 of individual trees per month for each category (flushing or abscission), we aggregated our
337 census to the monthly scale. Of the monitored trees, 69% ($n = 134$) had clear flushing and
338 abscission patterns, and, using the number of days after each flushing event, we determined
339 leaf age classes and attributed a fraction of the upper canopy crowns to an age class at
340 monthly intervals. We defined the following leaf age classes: (i) young leaves (0–1
341 month), (ii) growing (1–2 months), (iii) mature leaves (3–6 months), and (iv) old leaves
342 (>6 months). Then, we partitioned the age classes into classes of leaf area index (LAI)
343 (i.e., young, growing, mature, and old LAI) by normalizing each leaf age class with the
344 total LAI measured at ATTO. A constant LAI of $5.32 \text{ m}^2 \text{ m}^{-2}$ was used for all months,
345 since the variability of this number throughout the year was not statistically significant
346 (unpublished results). For the normalization, we considered the total number of trees in
347 the camera frame ($n = 194$), assuming that the 31% that do not have clear flushing patterns
348 are part of the old age class. For more details on the methods and assumptions for
349 separating LAI into leaf age classes, see Wu et al. (2016). Datasets of flushing and
350 abscission (<http://doi.org/10.17871/atto.223.7.840>) and the raw LAI age classes (<http://doi.org/10.17871/atto.230.4.842>).

351

352 353 2.8 Isoprene emission trait – tree species level

354

355 To get more detailed information on the trees monitored with the camera, a total of 194
356 trees were taxonomically identified, and the isoprene emission trait was assigned. Isoprene
357 emission data were obtained from published data and new measurements for the study
358 species. New measurements were conducted at the ATTO research site (described in
359 section 2.6), and additional measurements were obtained using the PORCO method (Taylor
360 et al., 2021), a customized photoionization detection system, on trees in tropical botanical
361 gardens. Briefly, all PORCO measurements were made in situ on uncut ‘sun’ branches by
362 enclosing one-to-few leaves inside rigid leaf cuvettes, acclimating them to darkness, and
363 then exposing the leaves to photosynthetically active radiation controlled at $1000 \mu\text{mol m}^{-2} \text{ s}^{-1}$,
364 and temperatures near 30°C , for 3.5 minutes of measurement time. Emission rates
365 were corrected to a 30°C equivalent based on a standard temperature response curve
366 (Guenther et al., 1993). Emission rates exceeding $1 \text{ nmol m}^{-2} \text{ s}^{-1}$ were considered positively
367 indicative of isoprene emissions. See the full method validation and a discussion of the
368 rarity of detection of other compounds as false positives for isoprene in Taylor et al. (2021).
369 Botanic gardens used for tree measurements were: A. Duque private collection, Retiro,

326 Antioquia, Colombia; Fairchild Tropical Botanical Garden, Miami, FL, USA; Jardín
 327 Botánico de Cartagena “Guillermo Piñeres”, Turbaco, Bolívar, Colombia; Jardín Botánico
 328 "Joaquín Antonio Uribe" de Medellín, Antioquia, Colombia; Montgomery Botanical
 329 Garden, Miami, FL, USA; Universidad Nacional de Medellín–Sede Medellín arboretum,
 330 Antioquia, Colombia.

331

332 For applying isoprene measurements from external datasets (botanic garden measurements
 333 or published literature) to our study species, we followed the methods of Taylor et al.,
 334 (2018, 2019). We used data compiled from 12 literature sources (Bracho-Nunez et al.,
 335 2013; Geron et al., 2002; Harley et al., 2004; Keller & Lerdau, 1999; Klinger et al., 1998;
 336 Klinger et al., 2002; Lerdau & Keller 1997; Padhy & Varshney, 2005; Tambunan et al.,
 337 2006; Taylor et al., 2018; Taylor et al., 2021; Varshney & Singh, 2003). Tree species
 338 taxonomy was standardized by the Taxonomic Name Resolution Service (Boyle et al.,
 339 2013; Boyle et al., 2021). We assigned species data only in terms of the genetically
 340 determined capacity to produce isoprene (Monson et al., 2013); we did not consider the
 341 variability in the strength of emissions, for which data are more limited and potentially
 342 confounded by method variation and species plasticity. A species-level emission status–
 343 emitter or non-emitter–was applied where available in external datasets; otherwise, genus-
 344 level information was used to impute the emission status to unmeasured species. The
 345 proportion of measured species in a genus that emit isoprene was used as an estimate of
 346 the probability (p_{IE}) that any species sampled from the genus would be an emitter. For a
 347 genus corresponding to one of our study species, for $p_{IE} \leq 1/3$, the species was estimated
 348 to be a non-emitter, and for $p_{IE} \geq 2/3$, the species was estimated to be an emitter. For values
 349 $1/3 < p_{IE} < 2/3$, the genus average was considered ambiguous and the species was excluded
 350 from the analyses. Whereas there is some expected error in the assignment of emission
 351 status to any given species, analyses of large numbers of species will tend toward the
 352 correct answer due to the tendency of genera to predominate in emitting or non-emitting
 353 species (Taylor et al., 2018). All species for which no emission data were available at the
 354 genus level were excluded from the analyses. The imputed isoprene emission status and
 355 associated information for each of our study species can be found in Table S2. The source
 356 data (literature reference or present study metadata) for each species that informed the
 357 imputation can be found in Table S3.

358

359 *2.9 Modeled isoprene flux estimates - Model of Emissions of Gases and Aerosols from* 360 *Nature (MEGAN)*

361

362 Isoprene fluxes were simulated using the MEGAN version 2.1 model in which the flux
 363 activity factor for isoprene (γ_i) is proportional to the emission response to light (γ_P),
 364 temperature (γ_T), leaf age (γ_A), soil moisture (γ_{SM}), leaf area index (LAI), and CO₂
 365 inhibition (γ_{CO_2}) according to Eq. (2) (Guenther et al., 2012):

366

$$367 \quad \gamma_i = C_{CE}LAI\gamma_P\gamma_T\gamma_A\gamma_{SM}\gamma_{CO_2} \quad (2)$$

368

369 For this study, the canopy environment model of Guenther et al. (2006) was used with a
 370 canopy environment coefficient (C_{CE}) of 0.57. MEGAN was run accounting for variations
 371 in light, temperature, and LAI separated into leaf age classes. CO₂ inhibition and soil

372 moisture activity factors were set equal to a constant of 1, assuming these parameters do
373 not vary. For all simulations, we assumed no seasonal variation in soil moisture because
374 the soil moisture observed in this site consistently exceeds the threshold for the isoprene
375 drought response in MEGAN 2.1 (Guenther et al., 2012), which means that MEGAN would
376 predict no variation in isoprene emission resulting from the observed changes in soil
377 moisture (Fig. 1).

378

379 Solar radiation (PPFD) and air temperature inputs for all model simulations were obtained
380 from measurements at the INSTANT tower. Air temperature at 36 m height above ground
381 level was measured with a temperature and relative humidity sensor (CS215-L, Campbell Scientific
382 Inc., Logan, Utah, USA). In cases where the air temperature measurement at 36 m height failed,
383 the missing data were gap-filled with air temperature data available at other heights (73 m, 55 m,
384 40 m, 12 m), measured with CS215-L sensors installed on the INSTANT tower, or with the air
385 temperature at 18 m above the ground measured with a thermocouple (Conatex, St. Wendel,
386 Germany), installed along one evergreen tree of the species *Buchenavia parvifolia* (*Combretaceae*),
387 located 95 m away from the INSTANT tower. In cases where all the air temperature sensors failed
388 for less than 4 hours, the missing air temperature at 36 m height was gap-filled by linear
389 interpolation, visually checking data quality. In cases where no air temperature measurement was
390 available for a long time (e.g., one day, 2 months etc.), confirmed several times in 2013, the missing
391 air temperature at 36 m height was gap-filled by a multiple regression model developed with three
392 predictor variables: half-hourly variation of the soil temperature at 10 cm depth, soil heat flux, and
393 volumetric soil water content at 40 cm depth. The model training period was from 2013 June to
394 2014 May because the three predictor variables were usually available through the one-year period.
395 The developed model was validated based on the observation dataset from June 2014 to May 2015,
396 which showed good agreement with observed air temperature data at 36 m height during the
397 validation period ($R^2 = 0.83$; $RMSE = 1.21$; $n = 7473$). The developed and validated model was
398 applied to the three predictor variables measured in 2013 for gap-filling the long-term missing data
399 of air temperature at 36 m height. In cases where the predictor variables were unavailable in 2013,
400 the missing data were gap-filled using Akima interpolation with visual data quality checks.
401 Incoming and outgoing shortwave radiation was measured with a net radiometer (NR- Lite2, Kipp
402 & Zonen, the Netherlands) at 75 m above ground. In cases where the radiation measurement failed
403 for no more than 1 hour, the missing radiation data were gap-filled by linear interpolation, visually
404 checking data quality. In cases where radiation data were unavailable for more than 1 hour, the
405 missing data were gap-filled by the mean diurnal course (over ± 15 -day) method. Lastly, we used
406 a constant value (5.32) for the LAI and normalized it with monthly leaf age fractions
407 obtained from the phenocam observations to derive the canopy leaf age for each month
408 (see section 2.6). More details on model settings are found in Guenther et al. (2012).

409

410

411 3. Results and Discussion

412

413 3.1 Observations of canopy isoprene mixing ratios

414

415 We observed intra- and inter-annual variability of isoprene mixing ratios in canopy profiles
416 from nine intensive campaigns from Nov 2012 to Oct 2015 (Fig. 2a and Table 1). Figure
417 2b shows the leaf area density profile measured around the INSTANT tower in Oct 2015
418 and the mean canopy height. In general, isoprene mixing ratios were higher during the dry-
419 to-wet transition season (Nov 2012) and the dry season (Aug 2014 and Oct 2015/El-niño

420 year) than the wet season (Feb and Mar in 2013 and 2014) and the wet-to-dry transition
421 season (Jun 2013); with an exception for the Sep 2013-dry season that showed values
422 comparable to the 2014-wet season, although still higher than the 2013-wet season.
423 Interestingly, mean isoprene mixing ratios in Oct 2015 (El-niño dry season) were slightly
424 higher than those observed in Aug 2014 and Sep 2013 (both dry seasons) but not higher
425 than those observed in Nov 2012 (dry-to-wet transition) (although this was variable and
426 not significant). Seasonal changes in isoprene mixing ratios and fluxes from central
427 Amazonia have already been reported and were related to variations in temperature, light
428 availability at the surface, and leaf phenology (Yáñez-Serrano et al., 2015; Alves et al.,
429 2016, 2018; Wei et al., 2018; Langford et al., 2022), but the assessment of inter-annual
430 variability of consecutive years including anomalous years was lacking. Considering the
431 increased air temperatures observed in the 2015-El-niño dry season (Fig. 1b) and the fact
432 that tropical plant species emit high amounts of isoprene at high temperatures (Harley et
433 al., 2004; Alves et al., 2014; Jardine et al., 2014, Garcia et al., 2019; Rodrigues et al., 2020),
434 one could expect considerably higher emission and thereby high air mixing ratios of
435 isoprene during this extreme year. However, the 2015-El-niño dry season might have been
436 stressful for plants, with the anomalous drought (see soil moisture reduction in Fig. 1 d)
437 likely offsetting the high-temperature stimulus on isoprene emission. This finding can be
438 supported by two studies performed on this study site. Firstly, isoprene emission measured
439 in hyperdominant tree species showed a reduction in emission from the wet to the dry
440 season with a compensating increase in emission of monoterpenes and sesquiterpenes that
441 have both temperature-dependent emissions, indicating that the reduction in isoprene
442 emission and the shift toward heavier compounds resulted from abiotic stresses (e.g.,
443 drought) during the dry season (Gomes Alves et al., 2022), which might be substantially
444 higher in an extreme El-niño year. Secondly, the anomalous post-drought leaf flush
445 observed in Feb-Mar 2016 suggested that trees flushed out new leaves to recover from the
446 stress suffered during the 2015-El-niño dry season (Gonçalves et al., 2020).

447
448 Another interesting result was the seasonal variation in the shape of the isoprene mixing
449 ratio profiles (Fig. 2a). In general, all wet seasons (Feb-Mar 2013/2014) and the wet-to-dry
450 transition season (Jun 2013) data showed a constant profile with no clear vertical gradient
451 of isoprene. On the other hand, the dry seasons (Sep 2013, Aug 2014, and Oct 2015)
452 showed maximum mixing ratios between 12 m and 24m, and the dry-to-wet transition
453 season (Nov 2012) presented a well-defined peak at 24 m. This variation in the shape of
454 the isoprene mixing ratio profiles likely resulted from changes in isoprene emission across
455 seasons. Even though isoprene mixing ratio profiles are a combination of emission and air
456 mixing, when we analyzed the Bowen ratio at 24 m (figure S2) and the potential
457 temperature profiles (4-81 m; figure S1) across seasons, we observed that in-canopy air
458 mixing and the atmospheric stability were similar among seasons. This implies that
459 changes in isoprene mixing ratio profiles were predominantly attributed to the increase in
460 emission in certain layers, mostly at the upper canopy, during the dry and dry-to-wet
461 transition seasons. Furthermore, we suggest that the process that results in variation in the
462 shape of isoprene mixing ratio profiles is a combination of variations in the canopy leaf
463 area density profile and canopy leaf age distribution throughout the year. The total amount
464 of LAI has a small variation over the year; still, the fractions of leaf ages that compose this
465 total LAI changes seasonally (Wu et al., 2016), as well as the shape of the canopy leaf area

466 density profile, with significant changes at the upper canopy (Martins Rosa, 2016). During
467 the wet-to-dry transition season (May-Jun) and the dry season (Jul- Oct), upper canopy
468 trees presented leaf abscission and leaf flushing (Lopes et al., 2016, Gonçalves et al., 2020),
469 and the maturing process on the following months toward the beginning of the wet season
470 (Nov-Jan) might translate into higher leaf area density at the upper canopy (Martins Rosa,
471 2016) and higher gross primary productivity (GPP) (Botía et al., 2022). This implies that
472 two processes might be simultaneously occurring: one is that when there are more leaves
473 at the upper canopy, less light penetrates the canopy, which might induce the maximum
474 isoprene emission at the upper canopy as observed in Nov 2012; the other one is that leaves
475 at the upper canopy can have higher photosynthesis rates and, consequently, a higher
476 isoprene emission factor when they are mature (Alves et al., 2014), and more mature leaves
477 and higher GPP were observed in this study site during the dry-to-wet transition season and
478 beginning of the wet season (Lopes et al., 2016; Gonçalves et al., 2020; Botía et al., 2022).
479

480 In addition, it has been suggested that seasonal variations in isoprene emissions could result
481 from a variation in the isoprene emission factor with leaf aging, but there were not enough
482 observational studies to support it in the Amazon (Alves et al., 2018). Therefore, in the
483 next section, we show for the first time in-situ observations of isoprene emission factor at
484 leaf-level with known leaf age and infer how this, together with variation in canopy leaf
485 age distribution, likely affected intra- and inter-annual variability in emission during
486 sequenced years.

487

488 3.2 Seasonal changes in the isoprene emission factor (E_s)

489

490 The isoprene emission factor (E_s ; parameter measured at $1000 \mu\text{mol m}^{-2} \text{s}^{-1}$ PAR, 30°C) of
491 an ecosystem is determined by the fraction of species that emits this compound and by
492 variations in the E_s magnitude within species. Such variations may be conditioned by leaf
493 phenological status (e.g., young leaves have no or low emission, and old leaves emit less
494 isoprene than mature leaves) and environment (e.g., sun-leaves have higher E_s than shade-
495 leaves) (Niinemets, 2016). We performed measurements of E_s from sun-adapted leaves
496 across different ages in 21 trees (from 20 tree species) located at the upper canopy and
497 around the tower, and values ranged from 0 to $3.52 \text{ mg m}^{-2} \text{ h}^{-1}$ (see all species and emission
498 values in table S1). Of these 21 trees, 60 % had isoprene emission detectable by our
499 analytical system (TD-GC-TOFMS), while the other 40% did not. To evaluate whether
500 the E_s changes with leaf aging, we calculated the E_s ratios of mature (3–6 months) to young
501 (0–1 month), growing (1–2 months), and old (>6 months) leaves within the same tree
502 individual. We observed that, for some trees, E_s can be reduced by half when leaves are
503 older than six months (Fig. 3 and table S1), but the average of all trees combined showed
504 a statistically significant E_s reduction of 36% in old leaves compared to mature leaves
505 (paired t-test, p-value <0.05).
506

507

508 As tropical species represent a mix of phenotypes with the predominance of non-deciduous
509 plants, it was impossible to sample all leaf age classes for all tree species measured.
510 Nevertheless, our dataset covers leaf ages from 15 to 578 days (table S1), and we observed
511 that all leaves measured at the young leaf age class did not show detectable isoprene
emission, and two leaves measured at the growing leaf age class showed emissions similar

512 to the mature leaf age class (Fig.3 and table S1). As our sampling did not cover a broad
513 range of leaf ages below 60 days, especially among isoprene emitters, to improve the
514 robustness of our analysis, we added another species that had the E_s measured from the leaf
515 flushing day until the 30th day (young class) and at 226-227 days (old class) in the
516 southwestern Amazonia (Kuhn et al., 2004b). With this tree species added, we calculated
517 that the emission activity of E_s of young (0–1 month) and old (>6 months) leaves were,
518 respectively, 1% and 64% of the E_s observed in growing (1–2 months) and mature leaves
519 (3–6 months) (paired t-test, p-value <0.05), and that there was no statistically significant
520 difference between growing and mature leaves (paired t-test, p-value >0.05) (Fig. 3 and
521 table S1).

522
523 Furthermore, we observed that emitter species from our dataset could be combined into
524 two qualitative emission categories – medium emitter and low emitter –, given their E_s
525 magnitude compared to other leaf-level measurements in Amazonia (see a detailed
526 compilation in Yañez-Serrano et al., 2020), and high emitter, with the data from the tree
527 species measured in southwestern Amazonia (Kuhn et al., 2004b) (Fig. 3). The maximum
528 E_s occurred in different leaf ages for each emitter category. Still, both high and medium
529 emitters had an E_s maximum before 150 days (mature). In contrast, the low emitter category
530 showed an E_s maximum in 295 days (old) for one species, but that was not statistically
531 significant when compared to all low emitter species (paired t-test, p-value >0.05).
532 Therefore, this indicates that species that emit considerable amounts of isoprene have
533 maximum E_s when their leaves are mature.

534
535 The variation of E_s across leaf ages is already known, also for tropical tree species (Kuhn
536 et al., 2004b; Alves et al., 2014); however, the quantification of these variations across
537 different species is still a challenge given the high biodiversity in the Amazonian rainforest,
538 and, although our results show the variation of E_s across leaf ages for more species than
539 previously reported, it is still necessary to further develop tools to upscale these results to
540 the ecosystem level. Earlier studies indicated that the capacity to emit isoprene is more
541 common, and the E_s magnitudes are expected to be the highest in deciduous tree species
542 (Harrison et al., 2013; Dani et al., 2014). In fact, the high emitter (Fig. 3) is a tropical
543 deciduous tree species with a large range of variation in E_s within 30 days after leaf flushing
544 and with the maximum E_s observed in mature leaves at the end of the dry season (Kuhn et
545 al., 2004b). However, the number of deciduous trees that have regular leaf abscission and
546 leaf flushing during the dry season in central Amazonia may represent less than 15% of the
547 whole tree assembly (Gonçalves et al., 2020), which means that the effect of high
548 variability in the E_s with leaf aging from those trees might be low at the ecosystem level,
549 especially when we compare it with the other trees that showed less variability in the E_s
550 (Fig. 3, table S1).

551
552 Furthermore, for Amazonian tree species, the categorization of phenological habits goes
553 beyond evergreen and deciduous. Here, with a dataset of 194 trees (Fig. 4, and table S2)
554 monitored with a phenocam for leaf phenology and demography from 2013 to 2018, we
555 derived: (i) the camera-based canopy leaf area index (LAI) separated into four leaf age
556 classes - young (≤ 1 month), growing (1-2 months), mature (3-6 months), and old (>6
557 months) (Fig. 4a); and (ii) four classes of phenology (phenotypes) - evergreen, semi-
558 evergreen, brevi-deciduous, and semi-brevideciduous (Fig. 4c), based on the frequency of

559 events of leaf abscission and leaf flushing (more details in Supplementary Information).
560 Then, we assigned the isoprene trait for these tree species with measurements and literature
561 data, and imputed the trait to non-measured species by following the method described in
562 Taylor et al. (2018) (Fig. 4 c). We observed that the isoprene trait did not have a higher
563 percentage within brevi-deciduous and semi-brevideciduous phenotypes, which have
564 regular and seasonal leaf abscission and leaf flushing. Instead, all phenotypes had a similar
565 fraction of isoprene emitters (Fig. 4c). This implies that leaf age is an important factor for
566 the magnitude of E_s regardless of phenotype.

567
568 Although we do not have enough data to infer the phenotypes for the species monitored at
569 the branch level, we observed that the leaf age distribution of the 36 trees (Fig. 4b) was
570 similar to the 194 trees monitored with the phenocam (Fig. 4a); and that the fraction of
571 isoprene emitters was also similar when measured (21 trees – 60% emitters; Fig. 3) and
572 non-measured (15 trees – 47% emitters) were combined (56% emitters) (Fig. 4d) and
573 compared to the phenocam trees (60% emitters) (Fig. 4c). Note that the tree species that
574 had no isoprene emission trait reported in the literature and did not fill the assumptions
575 necessary to input the trait, according to Taylor et al. (2018), were assigned with the
576 unknown flag (NA).

577
578 The similarity found in the seasonal leaf age distribution between the 194 trees monitored
579 by the phenocam and the 36 trees monitored at the branch level (Fig. 4) is in agreement
580 with the results presented by Gonçalves et al. (2020), which showed that the leaf phenology
581 and demography of the 194 trees are representative of the region of this study, by
582 comparing it to corresponding satellite vegetation indices retrieved from MODIS-MAIAC
583 (Multi-Angle Implementation of Atmospheric Correction). Also, this, together with the fact
584 that the isoprene trait distribution was similar among the scales (leaf level and upper
585 canopy), implies that the E_s variation with leaf age measured here can be used to optimize
586 model estimates for intra- and inter-annual isoprene emission.

587 588 *3.3 Modeling of isoprene emission*

589
590 We used MEGAN to estimate isoprene emissions for the periods that we have in-situ
591 observations of isoprene and model inputs without considerable gaps, i.e., the years 2014
592 and 2015. We performed four different simulations (Fig. 5 and Table 2). For our first
593 simulation (S1), we applied MEGAN default settings for tropical vegetation (Fig. 5c,d),
594 which means that we used the E_s assigned to the broadleaf evergreen tropical tree and the
595 broadleaf deciduous tropical tree that is equal to $7 \text{ mg m}^{-2} \text{ h}^{-1}$ (Guenther et al., 2012), half-
596 hourly averages of air temperature and PPFD data measured at the same tower as the
597 isoprene observations (Fig. 5a,b), and no change in the leaf age algorithm. For the second
598 simulation (S2), we used a modified leaf age algorithm by adding the monthly distribution
599 of the LAI separated into leaf age classes (young, growing, mature, and old) as described
600 in the section above (Fig. 5c,d).

601
602 For a direct comparison between observations and model simulations, we performed eddy
603 covariance (EC) isoprene flux measurements during 11 days during Nov 2015 and
604 compared them with the simulations (Fig. 6). The isoprene emission sensitivity to the PPFD
605 circadian cycle was well simulated by MEGAN when estimates were compared with EC

606 isoprene flux ($r^2=0.84$, p -value <0.01) (Fig. 6 g). However, MEGAN simulations (S1 and
607 S2) overestimated the magnitude of emissions when compared with EC isoprene flux
608 around noontime (Fig. 6b); S1 and S2 had a daily average flux 2.71 and 2.68 times higher
609 than EC isoprene flux ($p<0.01$), respectively (Fig. 6h). This overestimation was a result of
610 a high value for E_s in the model setup ($7 \text{ mg m}^{-2} \text{ h}^{-1}$). To support this finding, we calculated
611 E_s from the observed EC isoprene flux data from 06:00 to 18:00 with the G93 algorithm
612 (Guenther et al., 1993), and E_s resulted in $3.21 \pm 1.76 \text{ mg m}^{-2} \text{ h}^{-1}$. We then ran a third
613 simulation (S3) with the corrected E_s ($3.21 \text{ mg m}^{-2} \text{ h}^{-1}$) (Fig. 5c,d; Fig. 6b) and S3 estimates
614 presented a daily average flux 1.23 higher than EC isoprene flux ($p=0.013$) (Fig. 6b,h). The
615 mean E_s calculated from EC isoprene flux is in the same range as the E_s observed for the
616 leaf level emissions of 21 trees (Fig. 3 and table S1), indicating that E_s from this study site
617 is lower than the one set in the model default.

618

619 Another modification in the model was done based on our leaf-level measurements. In
620 section 3.2, we present the E_s variation across leaf ages and suggest that the seasonal
621 variation in canopy leaf age distribution results in an emergent property to canopy seasonal
622 variation in E_s . With the LAI separated into leaf age classes (phenocam data) along the year
623 and the ratios of E_s (leaf level measurements) between mature and young leaves, mature
624 and old leaves, and mature and growing leaves, we modified the leaf age emission activity
625 factor of the leaf age algorithm in MEGAN. The modified leaf age emission activity factor
626 accounts for lower values of E_s in young and old leaves compared to mature and growing
627 leaves (Table 2). In our fourth simulation (S4) (Fig. 5c,d; Fig. 6b), we added the
628 modification in the leaf age emission activity factor, which led to a daily average 1.15
629 higher than EC isoprene flux ($p=0.03$) (Fig. 6 h).

630

631 To evaluate the effectiveness of our modifications in the model on intra- and inter-annual
632 timescales, we compared the isoprene mixing ratios observed at 38m height in all
633 campaigns performed in 2014 and 2015 with the four simulations. As our observations,
634 except for Nov 2015, are mixing ratios, it is only possible to indirectly compare with
635 MEGAN using an atmospheric model. However, considering that: air mixing and
636 atmospheric stability were similar among the seasons (figures S2 and S3); isoprene
637 emission is primarily driven by changes in light, temperature, and leaf phenology (Alves
638 et al., 2018), and the variability of these factors was included in the model; we can still test
639 the comparability of the changes in the magnitudes from our measurements and simulations
640 that resulted from intra- and inter-annual variations. In figure 7, we show linear regressions
641 between observations and simulations. All datasets were filtered to the period between 12-
642 15h, local time, to evaluate the time of the day with maximum emission and high mixing
643 in the surface layer and to reduce variability in photochemical isoprene loss rates. Figure 7
644 shows that, apart from the slope, all simulations were similarly and significantly
645 comparable to observations ($r^2=0.41$ and $r^2=0.42$, $p \ll 0.01$). However, it is important to
646 note that the finding of observed reduced E_s , compared to the model default settings, and
647 its changing across leaf ages may have an important effect on isoprene intra-annual
648 variation. Therefore, we expect that if more isoprene flux data, especially from long-term
649 measurements, were available for comparison with our simulations, we could have more
650 significant results in comparing observations and the simulations with all modifications in
651 MEGAN (S4). Additionally, as significant day-to-day isoprene variability was observed -

652 also over other Amazon regions, with isoprene concentrations of similar magnitudes
653 occurring during both wet and dry seasons, likely resulting from the longer wet season
654 lifetimes of isoprene (Wells et al., 2022), long-term flux measurements could help by
655 offering a direct comparison between observations and modeling, and the possibility to
656 evaluate atmospheric chemical processes.

657
658 In general, the modifications for the E_s (S3 and S4) and the leaf age activity factor (S4)
659 improved the estimates because they account for biological factors that have intra- and
660 inter-annual variations in this study site (Gonçalves et al., 2020), which represent a major
661 source of uncertainty in MEGAN (Niinemets et al., 2010). In this light, the main
662 improvement presented here resulted from the E_s correction since our observations showed
663 that E_s was less than half of the value in the model default settings and that E_s varies
664 significantly among leaf ages. This is important because E_s is a crucial factor in determining
665 the magnitudes of emission of a specific site, which may vary substantially in Amazonia.
666 Although a long-term canopy flux measurement study in central Amazonia indicated that
667 E_s does not vary seasonally and argued that intra-annual changes in isoprene emission
668 resulted only from micrometeorological and LAI variations (Langford et al., 2022), other
669 studies in central Amazonia have shown that emission varies substantially in a relatively
670 small spatial scale and on topographic gradients (Gu et al., 2017; Batista et al., 2019); and,
671 more recently, leaf-level measurements have shown that E_s varies within tree species both
672 seasonally and spatially, in particular when these species occur in different forest types and
673 topography (Gomes Alves et al., 2022).

674
675 *3.4 Implications of intra- and inter-annual variabilities in isoprene emission for modeling*

676
677 Despite the high variability within seasons, our results showed significant changes between
678 seasons. Previous studies have shown the strong seasonality of isoprene emission in central
679 Amazonia, and we corroborate these studies that indicated changes in solar radiation,
680 temperature, and leaf phenology, as the important drivers of isoprene intra-annual
681 variability (e.g., Yáñez-Serrano et al., 2015; Alves et al., 2016, 2018). However, here we
682 further develop our understanding concerning the effect of leaf phenology, by suggesting
683 that there is seasonal variation in the ecosystem E_s resulting from changes in canopy leaf
684 age distribution, which may significantly contribute to the seasonality in the magnitude of
685 actual emission rates. This is supported by our leaf-level E_s measurements, which showed
686 significant differences among leaf ages, with maximum values for mature leaves, and by
687 our results on canopy leaf age distribution changes. Furthermore, it is important to note
688 that leaf-level E_s from Oct-Nov 2017 showed maximum values for mature leaves, and those
689 were similar to the canopy E_s measured in Nov 2015. Oct and Nov (dry season and dry-to-
690 wet transition seasons) are months with a substantially higher fraction of mature leaves in
691 the canopy compared to those from the wet and wet-to-dry transition seasons, meaning that
692 the highest values of E_s from mature leaves likely predominate the ecosystem E_s in Oct-
693 Nov. In this sense, understanding how the E_s changes over seasons due to leaf age
694 composition within LAI will considerably improve model estimates of intra-annual
695 variations in isoprene. However, more long-term measurements of canopy isoprene flux
696 are needed to test it.
697

698 Surprisingly, inter-annual variabilities were less pronounced than intra-annual variability
699 when comparing normal years with the 2015-El-niño year. Our air temperature
700 measurements showed a significant increase during the dry season of 2015-El-niño year
701 compared to normal years. On a larger scale, regional land surface temperature retrieved
702 by satellite showed an increase of up to + 4 °C from Oct to Dec 2015 in the Amazon basin
703 (Jiménez-Muñoz et al., 2016), and that was accompanied by a significant negative
704 maximum climatological water deficit in 43% of the whole Amazon rainforest (Aragão et
705 al., 2018). Such stresses were expected to provide a stimulus for isoprene emission, as it is
706 already largely known that isoprene emission can increase with increasing temperature and
707 that some studies have also shown that emissions increase after moderate drought (e.g.,
708 Werner et al., 2021, Byron et al., 2022). However, our results did not show a significant
709 increase in isoprene mixing ratios in Oct 2015 compared to the dry seasons of previous
710 years, indicating that emissions were lower in Oct 2015, with the isoprene mixing ratio
711 profiles unlikely affected by in-canopy air mixing changes as suggested by the in-canopy
712 atmospheric stability analysis (figure S3). Understanding mechanisms of intra- and inter-
713 annual variations in canopy emissions of isoprene is essential for predicting their influence
714 on atmospheric chemical-physical processes. For example, the contribution of isoprene as
715 a sink for hydroxyl radical (OH) varied seasonally (Nölscher et al., 2016); however, it did
716 not vary significantly when a normal year and the 2015-El-niño year were compared in this
717 study site (Pfannerstill et al., 2018), leading to the conclusion that these forests contributed
718 to the emission of other compounds to cope with the stress during the 2015-El-niño year,
719 resulting in an effect on the atmospheric oxidative capacity (Pfannerstill et al., 2021).

720

721 Some models predicted that higher temperatures and extended drought periods resulting
722 from climate change might increase global isoprene emissions (Pegoraro et al., 2006).
723 However, more recently, a synthesis of studies performed in the Amazon suggested that,
724 as the increase in temperature comes along with biomass loss given deforestation and forest
725 degradation, a decrease in isoprene emission from Amazonia may be expected (Yáñez-
726 Serrano et al., 2020). Interestingly, although isoprene mixing ratios were not considerably
727 higher in the dry season of the 2015-El-niño year, previous studies observed higher
728 monoterpene mixing ratios compared to other dry seasons (Yáñez-Serrano et al., 2018) and
729 even higher monoterpene mixing ratios in drier and warmer days of the 2015-El-niño dry
730 season (Pfannerstill et al., 2018). In addition, another study conducted in central Amazonia
731 reported that the heat in 2015/16 led to a shift in plant emissions to more reactive
732 monoterpenes such as β -ocimene and that at high temperatures, monoterpene emissions
733 can be decoupled from photosynthesis (Jardine et al., 2017). Recently, leaf-level E_s
734 measurements in hyperdominant tree species in this study site showed that photosynthesis
735 and isoprene decreased while monoterpenes and sesquiterpenes proportionally increased
736 in the dry season, suggesting that plants might have emitted heavier compounds to cope
737 with the stress caused by high temperatures and potentially drought (Gomes Alves et al.,
738 2022). We suggest that anomalies in isoprene emission during extreme years are less
739 expected than anomalies in emissions of monoterpenes and sesquiterpenes since plants may
740 also emit compounds from their storage pools when there is a limited carbon supply to
741 produce isoprene, as might be the case of plants reducing photosynthesis under heat and
742 drought stresses.

743

744 **Summary and conclusions**

745

746 Understanding mechanisms of intra- and inter-annual variations in canopy emissions of
747 isoprene from Amazonia is essential for predicting their influence on atmospheric
748 chemical-physical processes, especially when considering the role of Amazonia in the
749 global BVOC emission budget. Earlier studies presented seasonal isoprene emissions and
750 related them to the seasonality of temperature, solar radiation, and leaf phenology.
751 Nevertheless, to the best of our knowledge, this is the first study showing the E_s variation
752 across leaf ages for several Amazonian tree species and the first attempt to represent the
753 effect on seasonal isoprene flux with a model parameterization. Also, by comparing
754 observations of normal years to the extreme 2015-El-niño year, we were able to show that
755 isoprene emission does not substantially increase as a result of higher temperatures. We
756 suggest that the stress caused by elevated temperatures and droughts in extreme years might
757 reduce the isoprene temperature dependence, which is not currently well represented in
758 modeling.

759

760 Even though there are uncertainties related to measurements and model simulations, the
761 results presented here suggest that E_s varied seasonally and that this is a key factor in
762 improving model predictions. Additionally, previous studies showed that a distinguished
763 high monoterpene emission accompanies a non-pronounced increase in isoprene emission
764 in extreme years during the dry season at this study site, which is interesting to investigate
765 further since monoterpenes have higher reactivity in the atmosphere. Therefore, more
766 detailed and long-term measurements of isoprene and other BVOCs are encouraged to
767 improve our understanding of the intra- and inter-annual variability of BVOC emissions in
768 Amazonia, especially measurements that also account for biological factors that might
769 contribute to more mechanistic surface emission modeling and subsequently lead to better
770 predictions of atmospheric chemical-physical processes.

771

772 **Data availability**

773 Datasets are available upon request on <https://attodata.org>.

774

775

776 **Authors' contributions**

777 Eliane Gomes Alves has designed this study and performed the leaf-level measurements,
778 the statistical analysis of observational datasets, and the MEGAN simulations. Raoni
779 Santana and Cleo Quaresma have contributed to the analysis of the datasets of canopy
780 isoprene mixing ratios and of micrometeorology. Santiago Botía has contributed to the
781 analysis of the phenocam dataset and performed the MEGAN simulations. Tyeen Taylor
782 contributed new measurements of isoprene emissions from tropical tree species and the
783 imputation modeling of isoprene trait to the tree species monitored by the phenocam. Ana
784 Maria Yáñez-Serrano and Jürgen Kesselmeier have provided the canopy isoprene mixing
785 ratios dataset. Pedro Ivo Lembo Silveira de Assis and Giordane Martins have contributed
786 with the leaf age monitoring at the branch level. Rodrigo de Souza and Sergio Duvoisin
787 Junior contributed to the collection of isoprene samples measured at leaf-level. Alex
788 Guenther and Dasa Gu have contributed with the chemical analysis of isoprene samples
789 measured at leaf-level and the MEGAN simulations. Anywhere Tsokankunku, Matthias

790 Sörgel, Efstratios Bourtsoukidis, and Jonathan Williams contributed with the dataset of
791 eddy covariance isoprene flux. Bruce Nelson and Davieliton Pinto contributed to the
792 collection and the analysis of the phenocam dataset. Shujiro Komiya contributed to
793 analyzing the micrometeorology dataset to run the MEGAN simulations. Diogo Martins
794 contributed to the surface LiDAR data collection and analysis. Bettina Weber and Cybelli
795 Barbosa contributed with the temperature dataset to run the MEGAN simulations. Michelle
796 Robin contributed new measurements of isoprene emissions from tropical tree species.
797 Kenneth Feeley, Alvaro Duque, Viviana Lemos, Maria Contreras, Alvaro Idarraga,
798 Norberto Lopez, Chad Husby, and Brett Jestrow contributed expert guidance, specimen
799 curation, field assistance, and botanical identifications for isoprene measurements from
800 trees in botanic gardens and private collections. Iván Mauricio Cely Toro contributed to in-
801 canopy micrometeorology analysis. All authors contributed to the writing of the
802 manuscript.

803

804 **Competing interests**

805 The authors declare that they have no conflict of interest

806

807 **Acknowledgements**

808 We thank the National Institute of Amazonian Research (INPA) and the Max Planck
809 Institute for Biogeochemistry (MPI-BGC) for their continuous support. We acknowledge
810 the support by the ATTO project (German Federal Ministry of Education and Research,
811 BMBF funds 01LB1001A; Brazilian Ministry of Science, Technology, Innovation and
812 Communication; FINEP/MCTIC contract 01.11.01248.00); UEA and FAPEAM,
813 LBA/INPA and SDS/CEUC/RDS-Uatumã. TCT was supported by grant #NSF-PRFB-
814 1711997, and #NSF-1754163. We also truly thank Marta Sá and Paulo Ricardo Teixeira
815 for their work on checking the quality of the micrometeorology dataset and the INPA's
816 Microeteorology Lab for providing the dataset. We acknowledge the helpful support for
817 isoprene measurements in botanic gardens by Santiago Madriñan of the Jardín Botánico
818 "Guillermo Piñeres", Ana María Benavides and Juan David Fernandes of the Jardín
819 Botánico de Medellín, Carl Lewis and Chad Husby of the Fairchild Botanic Garden, and
820 Patrick Griffith, Joanna Tucker Lima, and Michelle Barros of the Montgomery Botanical
821 Garden. We would like to especially thank the field assistants and all the people involved
822 in the logistic support of the ATTO project, who were all imperative for the development
823 of this study. We also thank all the indigenous communities that have been bravely
824 protecting the forest, and the riverside communities that have always helped us to do our
825 science. Without the "mateiros" we could never accomplish our scientific goals.

826

827

828 **References**

829 Alves, E. G., Harley, P., Gonçalves, J. F. C., Moura, C. E. S., and Jardine, K.: Effects of
830 light and temperature on isoprene emission at different leaf developmental stages of
831 *Eschweilera coriacea* in central Amazon, *Acta Amazonica*, 44, 9–18,
832 <https://doi.org/10.1590/S0044-59672014000100002>, 2014.

833

834 Alves, E. G., Jardine, K., Tota, J., Jardine, A., Yáñez-Serrano, A. M., Karl, T., Tavares, J.,
835 Nelson, B., Gu, D., Stavrou, T., Martin, S., Artaxo, P., Manzi, A., and Guenther, A.:

- 836 Seasonality of isoprenoid emissions from a primary rainforest in central Amazonia, *Atmos*
837 *Chem Phys*, 16, 3903–3925, <https://doi.org/10.5194/acp-16-3903-2016>, 2016.
- 838
- 839 Alves, E. G., Tóta, J., Turnipseed, A., Guenther, A. B., Vega Bustillos, J. O. W., Santana,
840 R. A., Cirino, G. G., Tavares, J. v., Lopes, A. P., Nelson, B. W., de Souza, R. A., Gu, D.,
841 Stavrakou, T., Adams, D. K., Wu, J., Saleska, S., and Manzi, A. O.: Leaf phenology as one
842 important driver of seasonal changes in isoprene emissions in central Amazonia,
843 *Biogeosciences*, 15, 4019–4032, <https://doi.org/10.5194/bg-15-4019-2018>, 2018.
- 844
- 845 Andreae, M. O., Acevedo, O. C., Araújo, A., Artaxo, P., Barbosa, C. G. G., Barbosa, H.
846 M. J., Brito, J., Carbone, S., Chi, X., Cintra, B. B. L., da Silva, N. F., Dias, N. L., Dias-
847 Júnior, C. Q., Ditas, F., Ditz, R., Godoi, A. F. L., Godoi, R. H. M., Heimann, M., Hoffmann,
848 T., Kesselmeier, J., Könemann, T., Krüger, M. L., Lavric, J. v., Manzi, A. O., Lopes, A.
849 P., Martins, D. L., Mikhailov, E. F., Moran-Zuloaga, D., Nelson, B. W., Nölscher, A. C.,
850 Santos Nogueira, D., Piedade, M. T. F., Pöhlker, C., Pöschl, U., Quesada, C. A., Rizzo, L.
851 v., Ro, C. U., Ruckteschler, N., Sá, L. D. A., de Oliveira Sá, M., Sales, C. B., dos Santos,
852 R. M. N., Saturno, J., Schöngart, J., Sörgel, M., de Souza, C. M., de Souza, R. A. F., Su,
853 H., Targhetta, N., Tóta, J., Trebs, I., Trumbore, S., van Eijck, A., Walter, D., Wang, Z.,
854 Weber, B., Williams, J., Winderlich, J., Wittmann, F., Wolff, S., and Yáñez-Serrano, A.
855 M.: The Amazon Tall Tower Observatory (ATTO): Overview of pilot measurements on
856 ecosystem ecology, meteorology, trace gases, and aerosols, *Atmos Chem Phys*, 15, 10723–
857 10776, <https://doi.org/10.5194/acp-15-10723-2015>, 2015.
- 858
- 859 Aragão, L. E. O. C., Anderson, L. O., Fonseca, M. G., Rosan, T. M., Vedovato, L. B.,
860 Wagner, F. H., Silva, C. V. J., Silva Junior, C. H. L., Arai, E., Aguiar, A. P., Barlow, J.,
861 Berenguer, E., Deeter, M. N., Domingues, L. G., Gatti, L., Gloor, M., Malhi, Y., Marengo,
862 J. A., Miller, J. B., Phillips, O. L., and Saatchi, S.: 21st Century drought-related fires
863 counteract the decline of Amazon deforestation carbon emissions, *Nat Commun*, 9, 1–12,
864 <https://doi.org/10.1038/s41467-017-02771-y>, 2018.
- 865
- 866 Artaxo, P., Mohr, C., and Pöschl, U.: Tropical and Boreal Forest – Atmosphere
867 Interactions: A Review, 74, 24–163, <https://doi.org/https://doi.org/10.16993/tellusb.34>,
868 2022.
- 869
- 870 Atkinson, R.: Gas-Phase Tropospheric Chemistry of Volatile Organic Compounds: 1.
871 Alkanes and Alkenes, *J Phys Chem Ref Data*, 26, 215–290,
872 <https://doi.org/10.1063/1.556012>, 1997.
- 873
- 874 Barkley, M. P., Palmer, P. I., de Smedt, I., Karl, T., Guenther, A., and van Roozendaal, M.:
875 Regulated large-scale annual shutdown of Amazonian isoprene emissions?, *Geophys Res*
876 *Lett*, 36, L04803, <https://doi.org/10.1029/2008GL036843>, 2009.
- 877
- 878 Batista, C. E., Ye, J., Ribeiro, I. O., Guimarães, P. C., Medeiros, A. S. S., Barbosa, R. G.,
879 Oliveira, R. L., Duvoisin, S., Jardine, K. J., Gu, D., Guenther, A. B., McKinney, K. A.,
880 Martins, L. D., Souza, R. A. F., and Martin, S. T.: Intermediate-scale horizontal isoprene
881 concentrations in the near-canopy forest atmosphere and implications for emission

- 882 heterogeneity, *Proceedings of the National Academy of Sciences*, 116, 19318–19323,
883 <https://doi.org/10.1073/pnas.1904154116>, 2019.
- 884
- 885 Bauwens, M., Stavrakou, T., Müller, J. F., de Smedt, I., van Roozendaal, M., van der Werf,
886 G. R., Wiedinmyer, C., Kaiser, J. W., Sindelarova, K., and Guenther, A.: Nine years of
887 global hydrocarbon emissions based on source inversion of OMI formaldehyde
888 observations, *Atmos Chem Phys*, 16, 10133–10158, [https://doi.org/10.5194/acp-16-10133-](https://doi.org/10.5194/acp-16-10133-2016)
889 2016, 2016.
- 890
- 891 Botía, S., Komiya, S., Marshall, J., Koch, T., Gałkowski, M., Lavric, J., Gomes-Alves, E.,
892 Walter, D., Fisch, G., Pinho, D. M., Nelson, B. W., Martins, G., Luijkx, I. T., Koren, G.,
893 Florentie, L., Carioca de Araújo, A., Sá, M., Andreae, M. O., Heimann, M., Peters, W., and
894 Gerbig, C.: The CO₂ record at the Amazon Tall Tower Observatory: A new opportunity
895 to study processes on seasonal and inter-annual scales, *Glob Chang Biol*, 28, 588–611,
896 <https://doi.org/10.1111/gcb.15905>, 2022.
- 897
- 898 Boulton, C. A., Lenton, T. M., and Boers, N.: Pronounced loss of Amazon rainforest
899 resilience since the early 2000s, *Nat Clim Chang*, 12, 271–278,
900 <https://doi.org/10.1038/s41558-022-01287-8>, 2022.
- 901
- 902 Boyle, B., Hopkins, N., Lu, Z., Raygoza Garay, J. A., Mozzherin, D., Rees, T., Matasci,
903 N., Narro, M. L., Piel, W. H., Mckay, S. J., Lowry, S., Freeland, C., Peet, R. K., and
904 Enquist, B. J.: The taxonomic name resolution service: an online tool for automated
905 standardization of plant names, *BMC Bioinformatics*, 14, 16, [https://doi.org/10.1186/1471-](https://doi.org/10.1186/1471-2105-14-16)
906 2105-14-16, 2013.
- 907
- 908 Boyle, B. L., Matasci, N., Mozzherin, D., Rees, T., Barbosa, G. C., Kumar Sajja, R., &
909 Enquist, B. J. (2021). Taxonomic Name Resolution Service, version 5.0. In *Botanical*
910 *Information and Ecology Network*. <https://tnrs.biendata.org/>
- 911
- 912 Bracho-Nunez, A., Knothe, N. M., Welter, S., Staudt, M., Costa, W. R., Liberato, M. A.
913 R., Piedade, M. T. F., and Kesselmeier, J.: Leaf level emissions of volatile organic
914 compounds (VOC) from some Amazonian and Mediterranean plants, *Biogeosciences*, 10,
915 5855–5873, <https://doi.org/10.5194/bg-10-5855-2013>, 2013.
- 916
- 917 Byron, J.; Kreuzwieser, J.; Purser, G.; van Haren, J.; Ladd, S. N.; Meredith, L. K.; Werner,
918 C.; Williams, J.: Chiral monoterpenes reveal forest emission mechanisms and drought
919 responses, *Nature*, 609, 7926, <https://doi.org/10.1038/s41586-022-05020-5>, 2022.
- 920
- 921 Canaval, E., Millet, D. B., Zimmer, I., Nosenko, T., Georgii, E., Partoll, E. M., Fischer, L.,
922 Alwe, H. D., Kulmala, M., Karl, T., Schnitzler, J., and Hansel, A.: Rapid conversion of
923 isoprene photooxidation products in terrestrial plants, *Commun Earth Environ*, 1, 44,
924 <https://doi.org/10.1038/s43247-020-00041-2>, 2020.
- 925

- 926 Dani, K. G. S., Jamie, I. M., Prentice, I. C., and Atwell, B. J.: Evolution of isoprene
 927 emission capacity in plants, *Trends Plant Sci*, 19, 439–446,
 928 <https://doi.org/10.1016/j.tplants.2014.01.009>, 2014.
 929
- 930 Fauset, S., Johnson, M. O., Gloor, M., Baker, T. R., Monteagudo M., A., Brienen, R. J. W.,
 931 Feldpausch, T. R., Lopez-Gonzalez, G., Malhi, Y., ter Steege, H., Pitman, N. C. A.,
 932 Baraloto, C., Engel, J., Pétronelli, P., Andrade, A., Camargo, J. L. C., Laurance, S. G. W.,
 933 Laurance, W. F., Chave, J., Allie, E., Vargas, P. N., Terborgh, J. W., Ruokolainen, K.,
 934 Silveira, M., Aymard C., G. A., Arroyo, L., Bonal, D., Ramirez-Angulo, H., Araujo-
 935 Murakami, A., Neill, D., Hérault, B., Dourdain, A., Torres-Lezama, A., Marimon, B. S.,
 936 Salomão, R. P., Comiskey, J. A., Réjou-Méchain, M., Toledo, M., Licona, J. C., Alarcón,
 937 A., Prieto, A., Rudas, A., van der Meer, P. J., Killeen, T. J., Marimon Junior, B. H., Poorter,
 938 L., Boot, R. G. A., Stergios, B., Torre, E. V., Costa, F. R. C., Levis, C., Schiatti, J., Souza,
 939 P., Groot, N., Arets, E., Moscoso, V. C., Castro, W., Coronado, E. N. H., Peña-Claros, M.,
 940 Stahl, C., Barroso, J., Talbot, J., Vieira, I. C. G., van der Heijden, G., Thomas, R., Vos, V.
 941 A., Almeida, E. C., Davila, E. Á., Aragão, L. E. O. C., Erwin, T. L., Morandi, P. S., de
 942 Oliveira, E. A., Valadão, M. B. X., Zagt, R. J., van der Hout, P., Loayza, P. A., Pipoly, J.
 943 J., Wang, O., Alexiades, M., Cerón, C. E., Huamantupa-Chuquimaco, I., di Fiore, A.,
 944 Peacock, J., Camacho, N. C. P., Umetsu, R. K., de Camargo, P. B., Burnham, R. J., Herrera,
 945 R., Quesada, C. A., Stropp, J., Vieira, S. A., Steininger, M., Rodríguez, C. R., Restrepo, Z.,
 946 Muelbert, A. E., Lewis, S. L., Pickavance, G. C., and Phillips, O. L.: Hyperdominance in
 947 Amazonian forest carbon cycling, *Nat Commun*, 6, 1–9,
 948 <https://doi.org/10.1038/ncomms7857>, 2015.
 949
- 950 Fu, D., Millet, D. B., Wells, K. C., Payne, V. H., Yu, S., Guenther, A., and Eldering, A.:
 951 Direct retrieval of isoprene from satellite-based infrared measurements, *Nat Commun*, 10,
 952 3811, <https://doi.org/10.1038/s41467-019-11835-0>, 2019.
 953
- 954 Garcia, S., Jardine, K., de Souza, V. F., de Souza, R. A. F., Junior, S. D., and Gonçalves,
 955 J. F. de C.: Reassimilation of leaf internal CO₂ contributes to isoprene emission in the
 956 neotropical species *inga edulis* Mart, *Forests*, 10, <https://doi.org/10.3390/f10060472>, 2019.
 957 Geron, C., Guenther, A., Greenberg, J., Loescher, H. W., Clark, D., and Baker, B.: Biogenic
 958 volatile organic compound emissions from a lowland tropical wet forest in Costa Rica,
 959 *Atmos Environ*, 36, 3793–3802, [https://doi.org/10.1016/S1352-2310\(02\)00301-1](https://doi.org/10.1016/S1352-2310(02)00301-1), 2002.
 960 Gomes Alves, E., Taylor, T., Robin, M., Pinheiro Oliveira, D., Schiatti, J., Duvoisin Júnior,
 961 S., Zannoni, N., Williams, J., Hartmann, C., Gonçalves, J. F. C., Schöngart, J., Wittmann,
 962 F., and Piedade, M. T. F.: Seasonal shifts in isoprenoid emission composition from three
 963 hyperdominant tree species in central Amazonia, *Plant Biol*, 24, 721–733,
 964 <https://doi.org/10.1111/plb.13419>, 2022.
 965
- 966 Gonçalves, N., Pontes, A., Dalagnol, R., Wu, J., Mesquita, D., and Walker, B.: Remote
 967 Sensing of Environment Both near-surface and satellite remote sensing confirm drought
 968 legacy effect on tropical forest leaf phenology after 2015 / 2016 ENSO drought, *Remote
 969 Sens Environ*, 237, 111489, <https://doi.org/10.1016/j.rse.2019.111489>, 2020.
 970

- 971 Gu, D., Guenther, A. B., Shilling, J. E., Yu, H., Huang, M., Zhao, C., Yang, Q., Martin, S.
972 T., Artaxo, P., Kim, S., Seco, R., Stavrakou, T., Longo, K. M., Tóta, J., de Souza, R. A. F.,
973 Vega, O., Liu, Y., Shrivastava, M., Alves, E. G., Santos, F. C., Leng, G., and Hu, Z.:
974 Airborne observations reveal elevational gradient in tropical forest isoprene emissions, *Nat*
975 *Commun*, 8, <https://doi.org/10.1038/ncomms15541>, 2017.
976
- 977 Guenther, A., Nicholas, C., Fall, R., Klinger, L., Mckay, W. A., and Scholes, B.: A global
978 model of natural volatile organic compound emissions s Raja the balance Triangle changes
979 in the atmospheric accumulation rates of greenhouse Triangle Several inventories of
980 natural and Exposure Assessment global scales have been two classes Fores, *J. Geophys.*
981 *Res.*, 100, 8873–8892, 1995.
982
- 983 Guenther, A., Karl, T., Harley, P., Wiedinmyer, C., Palmer, P. I., and Geron, C.: Estimates
984 of global terrestrial isoprene emissions using MEGAN (Model of Emissions of Gases and
985 Aerosols from Nature), *Atmos Chem Phys*, 6, 3181–3210, [https://doi.org/10.5194/acpd-6-](https://doi.org/10.5194/acpd-6-107-2006)
986 [107-2006](https://doi.org/10.5194/acpd-6-107-2006), 2006.
987
- 988 Guenther, A. B. and Hills, A. J.: Eddy covariance measurement of isoprene fluxes, *Journal*
989 *of Geophysical Research Atmospheres*, 103, 13145–13152,
990 <https://doi.org/10.1029/97JD03283>, 1998.
991
- 992 Guenther, A. B., Zimmerman, P. R., Harley, P. C., Monson, R. K., and Fall, R.: Isoprene
993 and monoterpene emission rate variability - Model evaluation and sensitivity analyses.,
994 *Journal of Geophysical Research-Atmospheres*, 98, 12609–12617, 1993.
995
- 996 Guenther, A. B., Jiang, X., Heald, C. L., Sakulyanontvittaya, T., Duhl, T., Emmons, L. K.,
997 and Wang, X.: The Model of Emissions of Gases and Aerosols from Nature version 2.1
998 (MEGAN2.1): an extended and updated framework for modeling biogenic emissions,
999 *Geosci Model Dev*, 5, 1503–1560, <https://doi.org/10.5194/gmdd-5-1503-2012>, 2012.
1000
- 1001 Harley, P., Vasconcellos, P., Vierling, L., Pinheiro, C. C. D. S., Greenberg, J., Guenther,
1002 A., Klinger, L., Almeida, S. S. de, Neill, D., Baker, T., Phillips, O., and Malhi, Y.: Variation
1003 in potential for isoprene emissions among Neotropical forest sites, *Glob Chang Biol*, 10,
1004 630–650, <https://doi.org/10.1111/j.1529-8817.2003.00760.x>, 2004.
1005
- 1006 Harrison, S. P., Dani, K. G. S., Prentice, I. C., Atwell, B. J., Leishman, M. R., Medlyn, B.
1007 E., Wright, I. J., Morfopoulos, C., Arneth, A., Barkley, M. P., Loreto, F., Niinemets, Ü.,
1008 Possell, M., and Peñuelas, J.: Volatile isoprenoid emissions from plastid to planet, *New*
1009 *Phytologist*, 197, 49–57, <https://doi.org/10.1111/nph.12021>, 2013.
1010
- 1011 Holst, T., Arneth, A., Hayward, S., Ekberg, A., Mastepanov, M., Jackowicz-Korczynski,
1012 M., Friborg, T., Crill, P. M., and Backstrand, K.: BVOC ecosystem flux measurements at
1013 a high latitude wetland site, *Atmos Chem Phys*, 10, 1617–1634, 2010.
1014
- 1015 Jardine, K., Chambers, J., Alves, E. G., Teixeira, A., Garcia, S., Holm, J., Higuchi, N.,
1016 Manzi, A., Abrell, L., Fuentes, J. D., Nielsen, L. K., Torn, M. S., and Vickers, C. E.:

- 1017 Dynamic Balancing of Isoprene Carbon Sources Reflects Photosynthetic and
1018 Photorespiratory Responses to Temperature Stress, *Plant Physiol*, 166, 2051–2064,
1019 <https://doi.org/10.1104/pp.114.247494>, 2014.
1020
- 1021 Jardine, K. J., Jardine, A. B., Holm, J. A., Lombardozzi, D. L., Negron-Juarez, R. I., Martin,
1022 S. T., Beller, H. R., Gimenez, B. O., Higuchi, N., and Chambers, J. Q.: Monoterpene
1023 ‘thermometer’ of tropical forest-atmosphere response to climate warming, *Plant Cell*
1024 *Environ*, 40, 441–452, <https://doi.org/10.1111/pce.12879>, 2017.
1025
- 1026 Jensen, N. R., Gruening, C., Goded, I., Müller, M., Hjorth, J., and Wisthaler, A.: Eddy-
1027 covariance flux measurements in an Italian deciduous forest using PTR-ToF-MS, PTR-
1028 QMS and FIS, *Int J Environ Anal Chem*, 98, 758–788,
1029 <https://doi.org/10.1080/03067319.2018.1502758>, 2018.
1030
- 1031 Jiménez-Muñoz, J. C., Mattar, C., Barichivich, J., Santamaría-Artigas, A., Takahashi, K.,
1032 Malhi, Y., Sobrino, J. A., and Schrier, G. van der: Record-breaking warming and extreme
1033 drought in the Amazon rainforest during the course of El Niño 2015-2016,
1034 <https://doi.org/10.1038/srep33130>, 2016.
1035
- 1036 Karl, T., Potosnak, M., Guenther, A., Clark, D., Walker, J., Herrick, J. D., and Geron, C.:
1037 Exchange processes of volatile organic compounds above a tropical rain forest:
1038 Implications for modeling tropospheric chemistry above dense vegetation, *J Geophys Res*,
1039 109, D18306, <https://doi.org/10.1029/2004JD004738>, 2004.
1040
- 1041 Keller, M. and Lerdau, M.: Isoprene emission from tropical forest canopy leaves, *Global*
1042 *Biogeochem Cycles*, 13, 19–29, 1999.
1043
- 1044 Kesselmeier, J., Ciccioli, P., Kuhn, U., Stefani, P., Biesenthal, T., Rottenberger, S., Wolf,
1045 A., Vitullo, M., Valentini, R., Nobre, A., Kabat, P., and Andreae, M. O.: Volatile organic
1046 compound emissions in relation to plant carbon fixation and the terrestrial carbon budget,
1047 *Global Biogeochem Cycles*, 16, 73-1-73–9, <https://doi.org/10.1029/2001GB001813>, 2002.
1048 Klinger, L. F., Li, Q. J., Guenther, A. B., Greenberg, J. P., Baker, B., and Bai, J. H.:
1049 Assessment of volatile organic compound emissions from ecosystems of China, *J Geophys*
1050 *Res*, 107, 4603, <https://doi.org/10.1029/2001JD001076>, 2002.
1051
- 1052 Kljun, N., Calanca, P., Rotach, M. W., and Schmid, H. P.: A simple two-dimensional
1053 parameterisation for Flux Footprint Prediction (FFP), *Geosci Model Dev*, 8, 3695–3713,
1054 <https://doi.org/10.5194/gmd-8-3695-2015>, 2015.
1055
- 1056 Kuhn, U., Rottenberger, S., Biesenthal, T., Wolf, a., Schebeske, G., Ciccioli, P.,
1057 Brancaleoni, E., Frattoni, M., Tavares, T. M., and Kesselmeier, J.: Seasonal differences in
1058 isoprene and light-dependent monoterpene emission by Amazonian tree species, *Glob*
1059 *Chang Biol*, 10, 663–682, <https://doi.org/10.1111/j.1529-8817.2003.00771.x>, 2004a.
1060
- 1061 Kuhn, U., Rottenberger, S., Biesenthal, T., Wolf, A., Schebeske, G., Ciccioli, P., and
1062 Kesselmeier, J.: Strong correlation between isoprene emission and gross photosynthetic

- 1063 capacity during leaf phenology of the tropical tree species *Hymenaea courbaril* with
1064 fundamental changes in volatile organic compounds emission composition during early
1065 leaf development, *Plant Cell Environ*, 27, 1469–1485, [https://doi.org/10.1111/j.1365-](https://doi.org/10.1111/j.1365-3040.2004.01252.x)
1066 3040.2004.01252.x, 2004b.
- 1067
1068 Langford, B., House, E., Valach, A., Hewitt, C. N., Artaxo, P., Barkley, M. P., Brito, J.,
1069 Carnell, E., Davison, B., MacKenzie, A. R., Marais, E. A., Newland, M. J., Rickard, A. R.,
1070 Shaw, M. D., Yáñez-Serrano, A. M., and Nemitz, E.: Seasonality of isoprene emissions
1071 and oxidation products above the remote Amazon, *Environmental Science: Atmospheres*,
1072 2, 230–240, <https://doi.org/10.1039/D1EA00057H>, 2022.
- 1073
1074 Ler dau, M. and Keller, M.: Controls on isoprene emission from trees in a subtropical dry
1075 forest, *Plant Cell Environ*, 20, 569–578, [https://doi.org/10.1111/j.1365-](https://doi.org/10.1111/j.1365-3040.1997.00075.x)
1076 3040.1997.00075.x, 1997.
- 1077
1078 Lopes, A. P., Nelson, B. W., Wu, J., Graça, P. M. L. de A., Tavares, J. V., Prohaska, N.,
1079 Martins, G. A., and Saleska, S. R.: Leaf flush drives dry season green-up of the Central
1080 Amazon, *Remote Sens Environ*, 182, 90–98, <https://doi.org/10.1016/j.rse.2016.05.009>,
1081 2016.
- 1082
1083 Mauder, T. and Foken, T.: Documentation and Instruction Manual of the Eddy Covariance
1084 Software Package TK2, Bayreuth: Universität Bayreuth, 2004.
- 1085
1086 Monson, R. K., Jones, R. T., Rosenstiel, T. N., and Schnitzler, J. P.: Why only some plants
1087 emit isoprene, *Plant Cell Environ*, 36, 503–516, <https://doi.org/10.1111/pce.12015>, 2013.
- 1088 Niinemets, Ü.: Leaf age dependent changes in within-canopy variation in leaf functional
1089 traits: a meta-analysis, *J Plant Res*, 129, 313–338, [https://doi.org/10.1007/s10265-016-](https://doi.org/10.1007/s10265-016-0815-2)
1090 0815-2, 2016.
- 1091
1092 Niinemets, Ü.: Leaf age dependent changes in within-canopy variation in leaf functional
1093 traits: a meta-analysis, *J Plant Res*, 129, 313–338, [https://doi.org/10.1007/s10265-016-](https://doi.org/10.1007/s10265-016-0815-2)
1094 0815-2, 2016.
- 1095
1096 Niinemets, U., Monson, R. K., Arneth, A., Ciccioli, P., Kesselmeier, J., Kuhn, U., Noe, S.
1097 M., Penuelas, J., and Staudt, M.: The leaf-level emission factor of volatile isoprenoids:
1098 caveats, model algorithms, response shapes and scaling, *Biogeosciences*, 7, 1809–1832,
1099 <https://doi.org/10.5194/bg-7-1809-2010>, 2010.
- 1100
1101 Nobre, C. A., Sampaio, G., Borma, L. S., Castilla-Rubio, J. C., Silva, J. S., and Cardoso,
1102 M.: Land-use and climate change risks in the Amazon and the need of a novel sustainable
1103 development paradigm, *Proceedings of the National Academy of Sciences*, 113,
1104 <https://doi.org/10.1073/pnas.1605516113>, 2016.
- 1105
1106 Nölscher, A. C., Yáñez-Serrano, A. M., Wolff, S., de Araujo, A. C., Lavrič, J. v,
1107 Kesselmeier, J., and Williams, J.: Unexpected seasonality in quantity and composition of

- 1108 Amazon rainforest air reactivity, *Nat Commun*, 7, 10383,
1109 <https://doi.org/10.1038/ncomms10383>, 2016.
1110
- 1111 Padhy, P. K. and Varshney, C. K.: Isoprene emission from tropical tree species,
1112 *Environmental Pollution*, 135, 101–109, <https://doi.org/10.1016/j.envpol.2004.10.003>,
1113 2005.
1114
- 1115 Pegoraro, E., Rey, A., Abrell, L., Haren, J., and Lin, G.: Drought effect on isoprene
1116 production and consumption in Biosphere 2 tropical rainforest, *Glob Chang Biol*, 12, 456–
1117 469, <https://doi.org/10.1111/j.1365-2486.2006.01112.x>, 2006.
1118
- 1119 Pfannerstill, E. Y., Nölscher, A. C., Yáñez-Serrano, A. M., Bourtsoukidis, E., Keßel, S.,
1120 Janssen, R. H. H., Tsokankunku, A., Wolff, S., Sörgel, M., Sá, M. O., Araújo, A., Walter,
1121 D., Lavrič, J., Dias-Júnior, C. Q., Kesselmeier, J., and Williams, J.: Total OH Reactivity
1122 Changes Over the Amazon Rainforest During an El Niño Event, *Frontiers in Forests and*
1123 *Global Change*, 1, <https://doi.org/10.3389/ffgc.2018.00012>, 2018.
1124
- 1125 Pfannerstill, E. Y., Reijrink, N. G., Edtbauer, A., Ringsdorf, A., Zannoni, N., Araújo, A.,
1126 Ditas, F., Holanda, B. A., Sá, M. O., Tsokankunku, A., Walter, D., Wolff, S., Lavri, J. v.,
1127 Pöhlker, C., Sörgel, M., and Williams, J.: Total OH reactivity over the Amazon rainforest:
1128 Variability with temperature, wind, rain, altitude, time of day, season, and an overall budget
1129 closure, *Atmos Chem Phys*, 21, 6231–6256, <https://doi.org/10.5194/acp-21-6231-2021>,
1130 2021.
1131
- 1132 Pöhlker, C., Walter, D., Paulsen, H., Könemann, T., Rodríguez-caballero, E., Moran-
1133 zuloaga, D., Brito, J., Carbone, S., Degrendele, C., Després, V. R., Ditas, F., Pöhlker, M.
1134 L., Praß, M., Löbs, N., Saturno, J., Sörgel, M., Wang, Q., Weber, B., Wolff, S., Artaxo, P.,
1135 Pöschl, U., and Andreae, M. O.: Land cover and its transformation in the backward
1136 trajectory footprint region of the Amazon Tall Tower Observatory, 8425–8470, 2019.
1137
- 1138 Pöschl, U., Martin, S. T., Sinha, B., Chen, Q., Gunthe, S. S., Huffman, J. A., Borrmann, S.,
1139 Farmer, D. K., Garland, R. M., Helas, G., Jimenez, J. L., King, S. M., Manzi, A., Mikhailov,
1140 E., Pauliquevis, T., Petters, M. D., Prenni, A. J., Roldin, P., Rose, D., Schneider, J., Su, H.,
1141 Zorn, S. R., Artaxo, P., and Andreae, M. O.: Rainforest Aerosols as Biogenic Nuclei of
1142 Clouds and Precipitation in the Amazon, *Science* (1979), 329, 1513–1516,
1143 <https://doi.org/10.1126/science.1191056>, 2010.
1144
- 1145 Rodrigues, T. B., Baker, C. R., Walker, A. P., McDowell, N., Rogers, A., Higuchi, N.,
1146 Chambers, J. Q., and Jardine, K. J.: Stimulation of isoprene emissions and electron
1147 transport rates as key mechanisms of thermal tolerance in the tropical species *Vismia*
1148 *guianensis*, *Glob Chang Biol*, 26, 5928–5941, <https://doi.org/10.1111/gcb.15213>, 2020.
1149
- 1150 Sindelarova, K., Granier, C., Bouarar, I., Guenther, a., Tilmes, S., Stavrakou, T., Müller,
1151 J.-F., Kuhn, U., Stefani, P., and Knorr, W.: Global data set of biogenic VOC emissions
1152 calculated by the MEGAN model over the last 30 years, *Atmos Chem Phys*, 14, 9317–
1153 9341, <https://doi.org/10.5194/acp-14-9317-2014>, 2014.

- 1154
1155 Spirig, C., Neftel, A., Ammann, C., Dommen, J., Grabmer, W., Thielmann, A., Schaub,
1156 A., Beauchamp, J., Wisthaler, A., and Hansel, A.: Eddy covariance flux measurements of
1157 biogenic VOCs during ECHO 2003 using proton transfer reaction mass spectrometry,
1158 *Atmos Chem Phys*, 5, 465–481, <https://doi.org/10.5194/acp-5-465-2005>, 2005.
- 1159
1160 Stark, S. C., Leitold, V., Wu, J. L., Hunter, M. O., de Castilho, C. V., Costa, F. R. C.,
1161 McMahon, S. M., Parker, G. G., Shimabukuro, M. T., Lefsky, M. a, Keller, M., Alves, L.
1162 F., Schiatti, J., Shimabukuro, Y. E., Brandão, D. O., Woodcock, T. K., Higuchi, N., de
1163 Camargo, P. B., de Oliveira, R. C., Saleska, S. R., and Chave, J.: Amazon forest carbon
1164 dynamics predicted by profiles of canopy leaf area and light environment., *Ecol Lett*, 15,
1165 1406–14, <https://doi.org/10.1111/j.1461-0248.2012.01864.x>, 2012.
- 1166
1167 ter Steege, H., Pitman, N. C. A., Sabatier, D., Baraloto, C., Salomao, R. P., Guevara, J. E.,
1168 Phillips, O. L., Castilho, C. v, Magnusson, W. E., Molino, J.-F., Monteagudo, A., Nunez
1169 Vargas, P., Montero, J. C., Feldpausch, T. R., Coronado, E. N. H., Killeen, T. J.,
1170 Mostacedo, B., Vasquez, R., Assis, R. L., Terborgh, J., Wittmann, F., Andrade, A.,
1171 Laurance, W. F., Laurance, S. G. W., Marimon, B. S., Marimon, B.-H., Guimaraes Vieira,
1172 I. C., Amaral, I. L., Brienen, R., Castellanos, H., Cardenas Lopez, D., Duivenvoorden, J.
1173 F., Mogollon, H. F., Matos, F. D. de A., Davila, N., Garcia-Villacorta, R., Stevenson Diaz,
1174 P. R., Costa, F., Emilio, T., Levis, C., Schiatti, J., Souza, P., Alonso, A., Dallmeier, F.,
1175 Montoya, A. J. D., Fernandez Piedade, M. T., Araujo-Murakami, A., Arroyo, L., Gribel,
1176 R., Fine, P. V. A., Peres, C. A., Toledo, M., Aymard C., G. A., Baker, T. R., Ceron, C.,
1177 Engel, J., Henkel, T. W., Maas, P., Petronelli, P., Stropp, J., Zartman, C. E., Daly, D., Neill,
1178 D., Silveira, M., Paredes, M. R., Chave, J., Lima Filho, D. de A., Jorgensen, P. M., Fuentes,
1179 A., Schongart, J., Cornejo Valverde, F., di Fiore, A., Jimenez, E. M., Penuela Mora, M. C.,
1180 Phillips, J. F., Rivas, G., van Andel, T. R., von Hildebrand, P., Hoffman, B., Zent, E. L.,
1181 Malhi, Y., Prieto, A., Rudas, A., Ruschell, A. R., Silva, N., Vos, V., Zent, S., Oliveira, A.
1182 A., Schutz, A. C., Gonzales, T., Trindade Nascimento, M., Ramirez-Angulo, H., Sierra, R.,
1183 Tirado, M., Umana Medina, M. N., van der Heijden, G., Vela, C. I. A., Vilanova Torre, E.,
1184 Vriesendorp, C., et al.: Hyperdominance in the Amazonian Tree Flora, *Science* (1979),
1185 342, 1243092–1243092, <https://doi.org/10.1126/science.1243092>, 2013.
- 1186
1187 Tambunan, P., Baba, S., Kuniyoshi, A., Iwasaki, H., Nakamura, T., Yamasaki, H., and
1188 Oku, H.: Isoprene emission from tropical trees in Okinawa Island, Japan, *Chemosphere*,
1189 65, 2138–2144, <https://doi.org/10.1016/j.chemosphere.2006.06.013>, 2006.
- 1190
1191 Taylor, T. C., McMahon, S. M., Smith, M. N., Boyle, B., Violle, C., van Haren, J., Simova,
1192 I., Meir, P., Ferreira, L. v., de Camargo, P. B., da Costa, A. C. L., Enquist, B. J., and
1193 Saleska, S. R.: Isoprene emission structures tropical tree biogeography and community
1194 assembly responses to climate, *New Phytologist*, 220, 435–446,
1195 <https://doi.org/10.1111/nph.15304>, 2018.
- 1196
1197 Taylor, T. C., Smith, M. N., Slot, M., and Feeley, K. J.: The capacity to emit isoprene
1198 differentiates the photosynthetic temperature responses of tropical plant species, *Plant Cell*
1199 *Environ*, 42, 2448–2457, <https://doi.org/10.1111/pce.13564>, 2019.

- 1200
1201 Taylor, T. C., Wisniewski, W. T., Alves, E. G., Oliveira Junior, R. C., and Saleska, S. R.:
1202 A New Field Instrument for Leaf Volatiles Reveals an Unexpected Vertical Profile of
1203 Isoprenoid Emission Capacities in a Tropical Forest, *Frontiers in Forests and Global*
1204 *Change*, 4, 1–22, <https://doi.org/10.3389/ffgc.2021.668228>, 2021.
- 1205
1206 Varshney, C. K. and Singh, A. P.: Isoprene emission from Indian trees, *J Geophys Res*,
1207 108, 4803, <https://doi.org/10.1029/2003JD003866>, 2003.
- 1208
1209 Vickers, D. and Mahrt, L.: Quality control and flux sampling problems for tower and
1210 aircraft data, *J Atmos Ocean Technol*, 14, 512–526, <https://doi.org/10.1175/1520->
1211 [0426\(1997\)014<0512:QCAFSP>2.0.CO;2](https://doi.org/10.1175/1520-0426(1997)014<0512:QCAFSP>2.0.CO;2), 1997.
- 1212
1213 Wei, D., Fuentes, J. D., Gerken, T., Chamecki, M., Trowbridge, A. M., Stoy, P. C., Katul,
1214 G. G., Fisch, G., Acevedo, O., Manzi, A., von Randow, C., and dos Santos, R. M. N.:
1215 Environmental and biological controls on seasonal patterns of isoprene above a rain forest
1216 in central Amazonia, *Agric For Meteorol*, 256–257, 391–406,
1217 <https://doi.org/10.1016/j.agrformet.2018.03.024>, 2018.
- 1218
1219 Wells, K. C., Millet, D. B., Payne, V. H., Vigouroux, C., Aquino, C. A. B., Mazière, M.,
1220 Gouw, J. A., Graus, M., Kurosu, T., Warneke, C., and Wisthaler, A.: Next-Generation
1221 Isoprene Measurements From Space: Detecting Daily Variability at High Resolution,
1222 *Journal of Geophysical Research: Atmospheres*, 127,
1223 <https://doi.org/10.1029/2021JD036181>, 2022.
- 1224
1225 Werner, C., Meredith, L. K., Ladd, S. N., Ingrisich, J., Kübert, A., van Haren, J., Bahn, M.,
1226 Bailey, K., Bamberger, I., Beyer, M., Blomdahl, D., Byron, J., Daber, E., Deleeuw, J.,
1227 Dippold, M. A., Fudyma, J., Gil-Loaiza, J., Honeker, L. K., Hu, J., Huang, J., Klüpfel, T.,
1228 Krechmer, J., Kreuzwieser, J., Kühnhammer, K., Lehmann, M. M., Meeran, K., Misztal,
1229 P. K., Ng, W.-R., Pfannerstill, E., Pugliese, G., Purser, G., Roscioli, J., Shi, L., Tfaily, M.,
1230 and Williams, J.: Ecosystem fluxes during drought and recovery in an experimental forest,
1231 *Science* (1979), 374, 1514–1518, <https://doi.org/10.1126/science.abj6789>, 2021.
- 1232
1233 Wu, J., Albert, L. P., Lopes, A. P., Restrepo-Coupe, N., Hayek, M., Wiedemann, K. T.,
1234 Guan, K., Stark, S. C., Christoffersen, B., Prohaska, N., Tavares, J. v., Marostica, S.,
1235 Kobayashi, H., Ferreira, M. L., Campos, K. S., Silva, R. da Brando, P. M., Dye, D. G.,
1236 Huxman, T. E., Huete, A. R., Nelson, B. W., and Saleska, S. R.: Leaf development and
1237 demography explain photosynthetic seasonality in Amazon evergreen forests, *Science*
1238 (1979), 351, 972–976, <https://doi.org/10.1126/science.aad5068>, 2016.
- 1239
1240 Yáñez-Serrano, A. M., Nölscher, A. C., Williams, J., Wolff, S., Alves, E., Martins, G. A.,
1241 Bourtsoukidis, E., Brito, J., Jardine, K., Artaxo, P., and Kesselmeier, J.: Diel and seasonal
1242 changes of biogenic volatile organic compounds within and above an Amazonian
1243 rainforest, *Atmos Chem Phys*, 15, 3359–3378, <https://doi.org/10.5194/acp-15-3359-2015>,
1244 2015.
- 1245

1246 Yáñez-Serrano, A. M., Nölscher, A. C., Bourtsoukidis, E., Gomes Alves, E., Ganzeveld,
1247 L., Bonn, B., Wolff, S., Sa, M., Yamasoe, M., Williams, J., Andreae, M. O., and
1248 Kesselmeier, J.: Monoterpene chemical speciation in the Amazon tropical rainforest:
1249 variation with season, height, and time of day at the Amazon Tall Tower Observatory
1250 (ATTO), *Atmos Chem Phys*, 18, 3403–3418, <https://doi.org/10.5194/acp-2017-817>, 2018.

1251
1252 Yáñez-Serrano, A. M., Bourtsoukidis, E., Alves, E. G., Bauwens, M., Stavrakou, T., Llusà,
1253 J., Filella, I., Guenther, A., Williams, J., Artaxo, P., Sindelarova, K., Doubalova, J.,
1254 Kesselmeier, J., and Peñuelas, J.: Amazonian biogenic volatile organic compounds under
1255 global change, *Glob Chang Biol*, 26, 4722–4751, <https://doi.org/10.1111/gcb.15185>, 2020.

1256
1257 Zannoni, N., Leppla, D., Lembo Silveira de Assis, P. I., Hoffmann, T., Sá, M., Araújo, A.,
1258 and Williams, J.: Surprising chiral composition changes over the Amazon rainforest with
1259 height, time and season, *Commun Earth Environ*, 1, 1–11, <https://doi.org/10.1038/s43247-020-0007-9>, 2020.

1261

1262

1263

1264 Tables

1265

1266 **Table 1.** Isoprene mixing ratios (ppbv) at 38 m for all field campaigns. Mixing ratios are
1267 mean values of isoprene measured at 12:00-15:00, local time (UTC-4h). Values within
1268 brackets are one standard deviation of the mean and the number of sampling days for each
1269 campaign.

Year	Month	Season	Isoprene (ppbv) at 38 m
2012	November	dry-to-wet transition season	9.30 (4.90) (n=4 days)
2013	February	wet season	1.10 (0.66) (n=6 days)
2013	March	wet season	1.84 (1.44) (n=3 days)
2013	June	wet-to-dry transition season	1.83 (0.82) (n=5 days)
2013	September	dry season	5.02 (1.99) (n=8 days)
2014	February	wet season	5.92 (4.89) (n=3 days)
2014	March	wet season	2.92 (2.50) (n=11 days)
2014	August	dry season	7.76 (2.49) (n=15 days)
2015	October	dry season – <i>El-Niño</i> year	8.94 (1.41) (n=13 days)

1270

1271

1272

1273

1274

1275

1276

1277

1278

1279

1280 **Table 2.** Model parameters for all simulations for the years 2014 and 2015.

	1 st model simulation (S1)	2 nd model simulation (S2)	3 rd model simulation (S3)	4 th model simulation (S4)
PPFD and air temperature	30 min averages – tower measurements	30 min averages – tower measurements	30 min averages – tower measurements	30 min averages – tower measurements
β^1	0.13	0.13	0.13	0.13
LDF ²	1	1	1	1
C_{t1}^3	95	95	95	95
C_{co}^4	2	2	2	2
Isoprene emission factor (E_s)	7 mg m ⁻² h ⁻¹	7 mg m ⁻² h ⁻¹	3.21 mg m ⁻² h ⁻¹	3.21 mg m ⁻² h ⁻¹
LAI	5.32	5.32	5.32	5.32
Leaf age algorithm – LAI	default	Modified with leaf age classes derived from the phenocam: <i>young leaves (0–1 month), growing (1–2 months), mature leaves (3–6 months), old leaves (>6 months).</i>	Modified with leaf age classes derived from the phenocam: <i>young leaves (0–1 month), growing (1–2 months), mature leaves (3–6 months), old leaves (>6 months).</i>	Modified with leaf age classes derived from the phenocam: <i>young leaves (0–1 month), growing (1–2 months), mature leaves (3–6 months), old leaves (>6 months).</i>
Leaf age emission activity factor	default $A_{new}=0.05$ $A_{gro}=0.6$ $A_{mat}=1$ $A_{old}=0.9$	default $A_{new}=0.05$ $A_{gro}=0.6$ $A_{mat}=1$ $A_{old}=0.9$	default $A_{new}=0.05$ $A_{gro}=0.6$ $A_{mat}=1$ $A_{old}=0.9$	modified according to leaf-level measurements: $A_{new}=0.01$ $A_{gro}=1$ $A_{mat}=1$ $A_{old}=0.64$

1281 *Note:* Empirical coefficients are from Guenther et al. (2012)

1282 1. Temperature empirical coefficient

1283 2. Light-dependent fraction

1284 3. Temperature empirical coefficient

1285 4. Emission-class dependent empirical coefficient

1286

1287

1288

1289

1290

1291

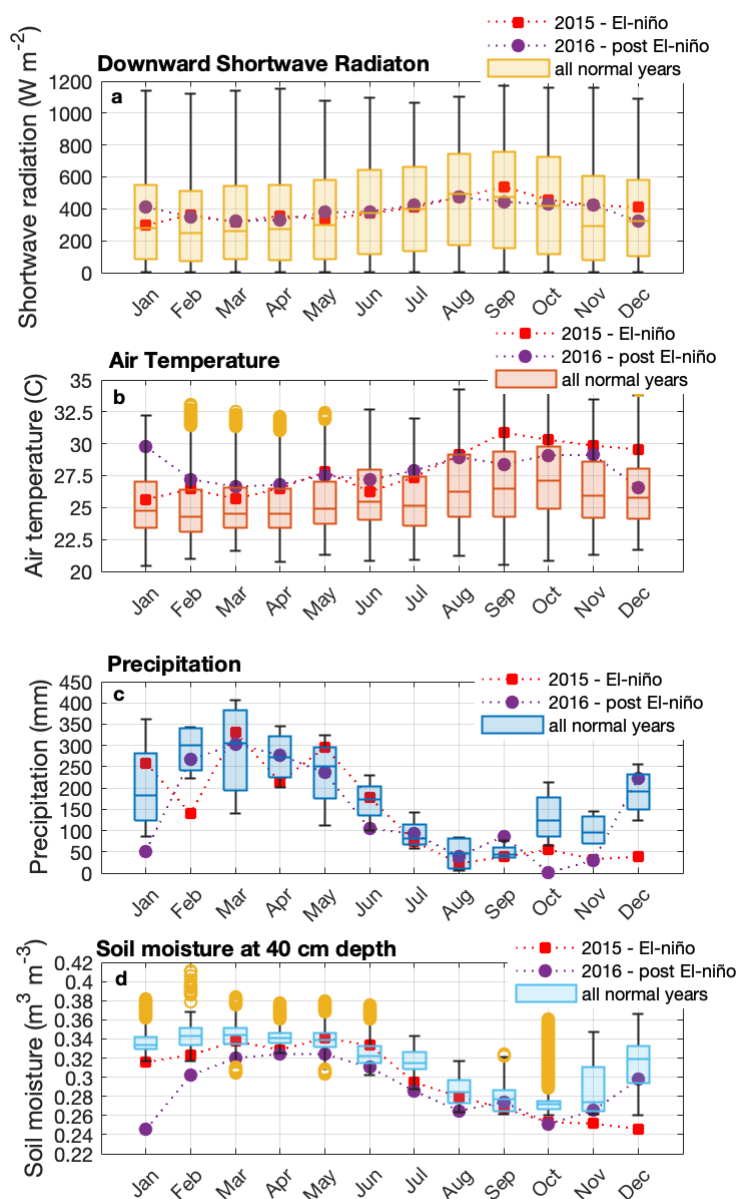
1292

1293

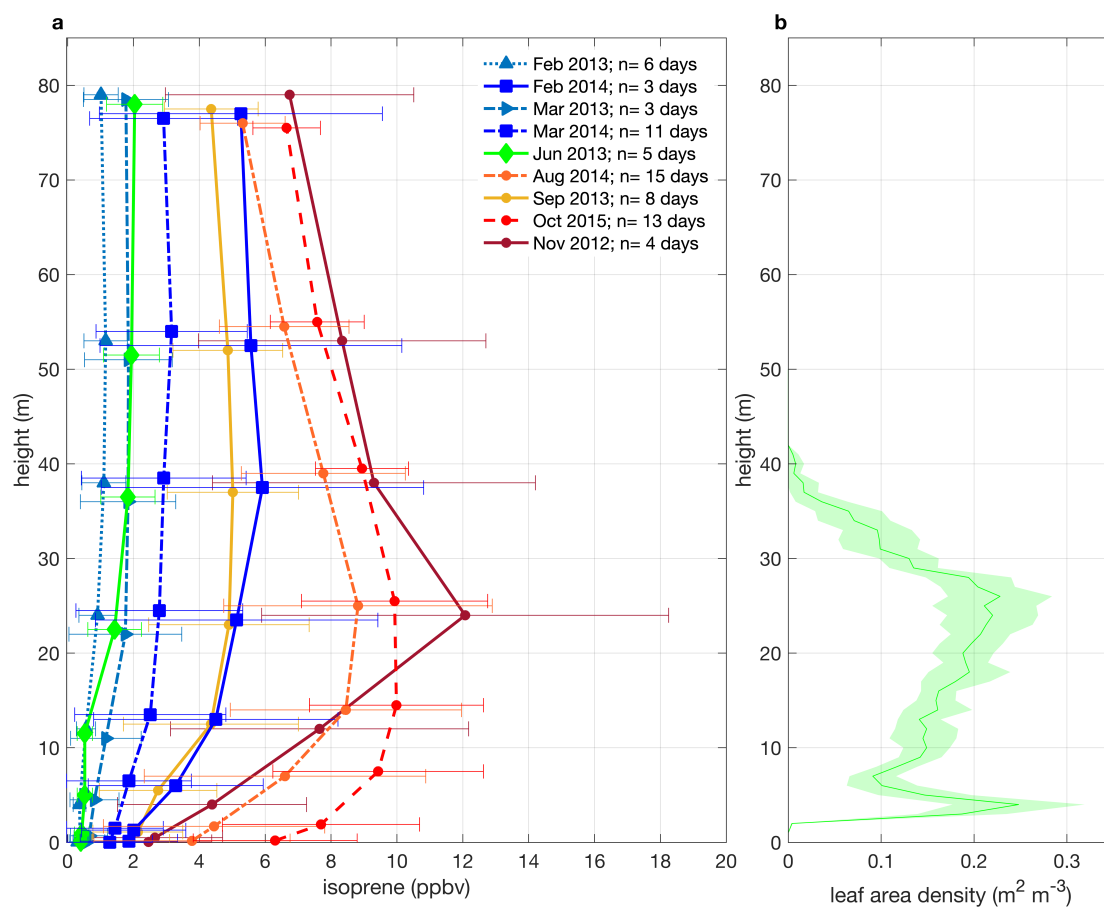
1294

1295

1296 **Figures**
 1297

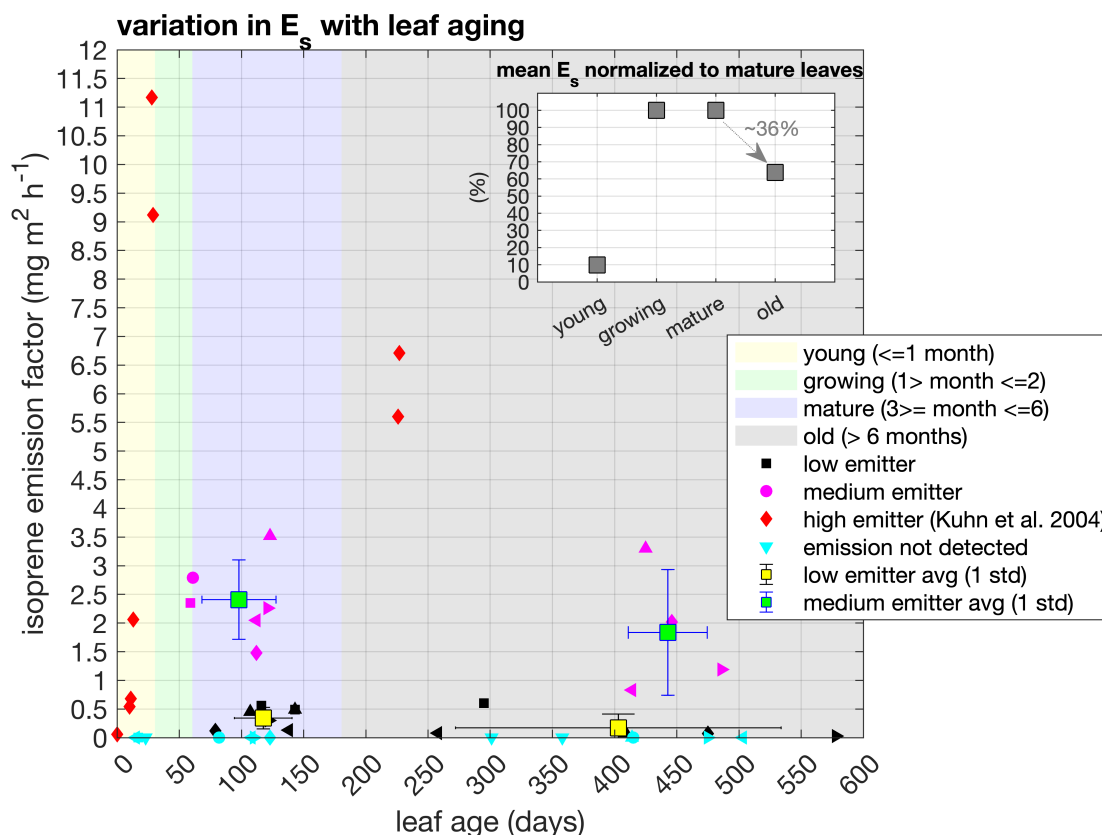


1298
 1299 **Figure 1.** Seasonal variation of solar radiation (a), air temperature (b), precipitation (c), and soil
 1300 moisture (d) during normal years (2013, 2014, 2017, 2018, and 2019), an El-niño (2015), and post-
 1301 El-niño year (2016) - measured at the ATTO site. Boxplots present the median, the lower, and the
 1302 upper quartiles, where the upper quartile corresponds to the 0.75 quantile and the lower quartile
 1303 corresponds to the 0.25 quantile; whiskers connect the upper quartile and lower quartile to the
 1304 maximum and minimum nonoutliers, respectively; and outliers are values that are more than
 1305 $1.5 \cdot IQR$ (interquartile range) away from the top or bottom of the box.
 1306
 1307
 1308
 1309
 1310



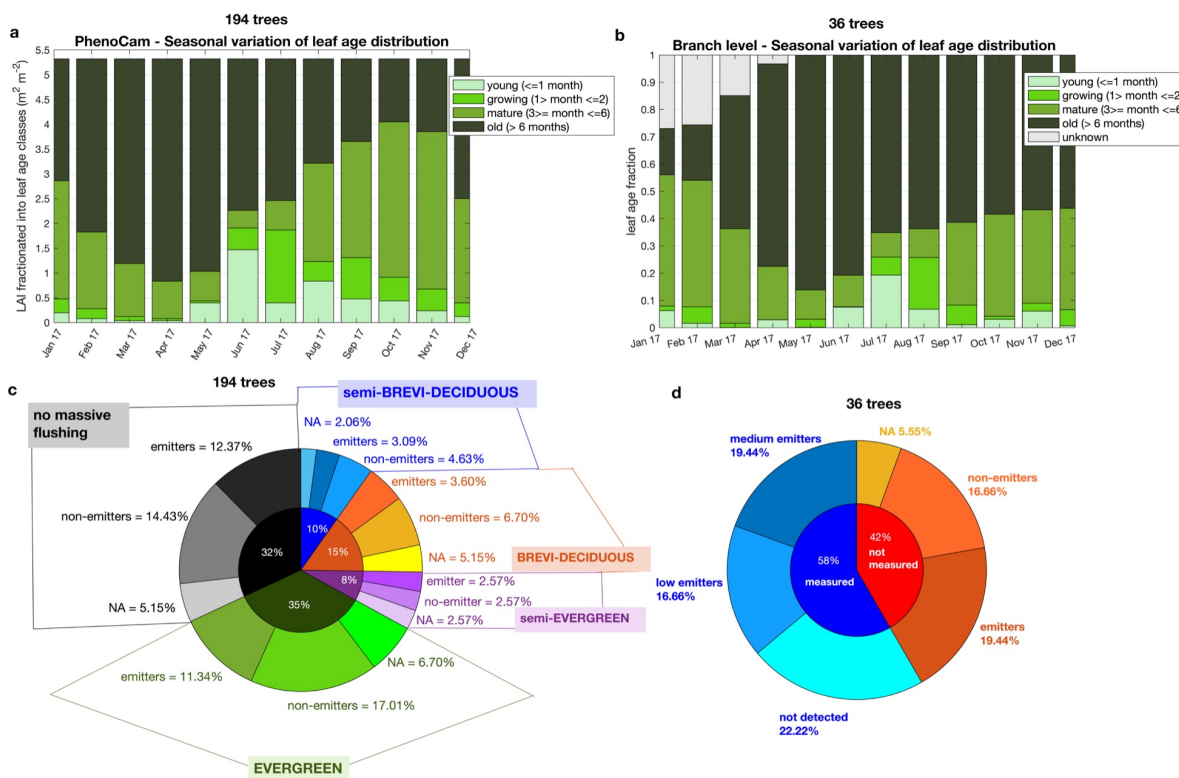
1311
 1312 **Figure 2.** Mean isoprene mixing ratios for all field campaigns from Nov 2012 to Oct
 1313 2015, with one standard deviation - 12:00-15:00 local time, UTC-4h - a daytime period
 1314 that isoprene emission is the highest; and mean canopy leaf area density profile with a
 1315 confidence interval of 95% (b). The measurements of all intensive campaigns were
 1316 collected at the same heights (0.05, 0.5, 4, 12, 24, 38, 53, and 79 m), but note that in the
 1317 plot (a), the heights were shifted by 50 cm only for the better visualization of the error
 1318 bars.

1319
 1320
 1321
 1322
 1323
 1324
 1325
 1326
 1327
 1328
 1329
 1330
 1331

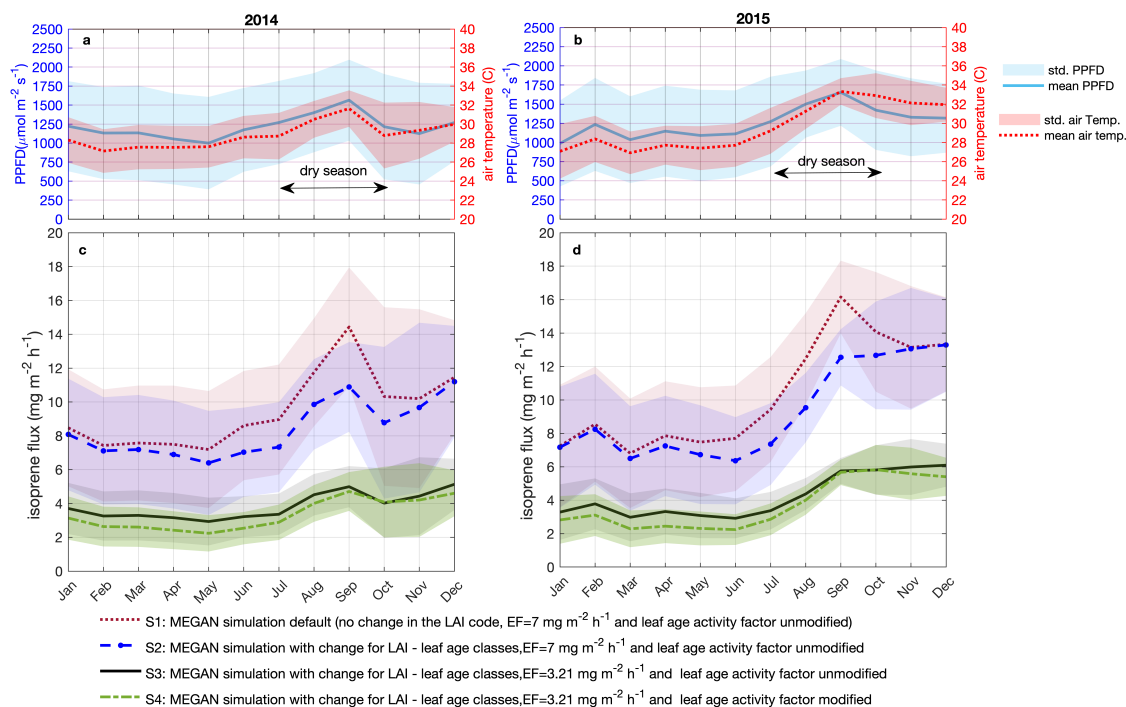


1332
 1333 **Figure 3.** Isoprene emission factor (E_s) across leaf age classes and characterized into
 1334 qualitative emission categories – low, medium, and high. Measured tree species were
 1335 categorized into medium (blue) and low (black) emitters according to their E_s values, and
 1336 different symbols represent different tree species. The high emitter category (red)
 1337 represents a tropical species measured in Kuhn et al. (2004b). Values represent
 1338 observations of individual trees and mean and one standard deviation for the categories
 1339 medium and low emitters at mature and old leaf age classes. Shade areas represent the
 1340 intervals of days for each leaf age class. The inset figure shows the mean E_s ratios of mature
 1341 (3-6 months) to young (0-1 month), growing (1-2 months), and old (> 6 months) leaves
 1342 calculated from the ratio of each individual tree.

1343
 1344
 1345
 1346
 1347
 1348
 1349
 1350
 1351
 1352
 1353
 1354
 1355
 1356

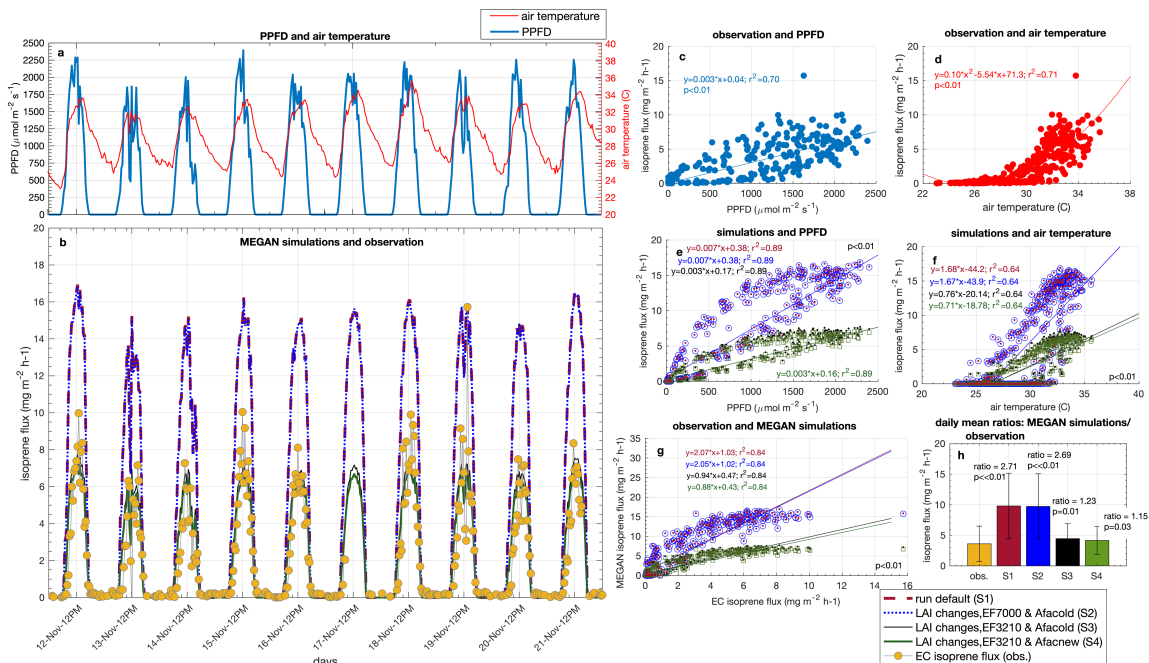


1357
1358 **Figure 4.** Leaf phenology and demography and isoprene emission trait. Panel (a) shows the leaf
1359 age distribution separated into LAI that was observed with the phenocam, in 2017; and panel (b)
1360 shows the leaf age distribution observed at branch level for 36 trees, in 2017 - note that unknown
1361 age refers to leaves that were attached to the branch at the beginning of monitoring and therefore
1362 could not be assigned to an age class. Panel (c) shows the percentual distribution of the phenotypes
1363 assigned to the 194 trees observed with the phenocam – no massive flushing, evergreen, semi-
1364 evergreen, deciduous, and semi-breveideciduous –, and the emission trait assigned to each tree
1365 species within these phenotypes – emitters, non-emitters, and NA (NA=no data available). Panel
1366 (d) presents the percentual distribution of the isoprene trait estimated to the non-measured trees
1367 (red); and the isoprene emission trait within measured tree species (blue), with measured tree
1368 species being categorized in classes of medium emission, low emission and not detected emission.
1369
1370
1371
1372
1373
1374
1375
1376
1377
1378
1379
1380
1381
1382
1383
1384



1385
 1386
 1387
 1388
 1389
 1390
 1391
 1392
 1393
 1394
 1395
 1396
 1397
 1398
 1399
 1400
 1401
 1402
 1403
 1404
 1405
 1406
 1407
 1408

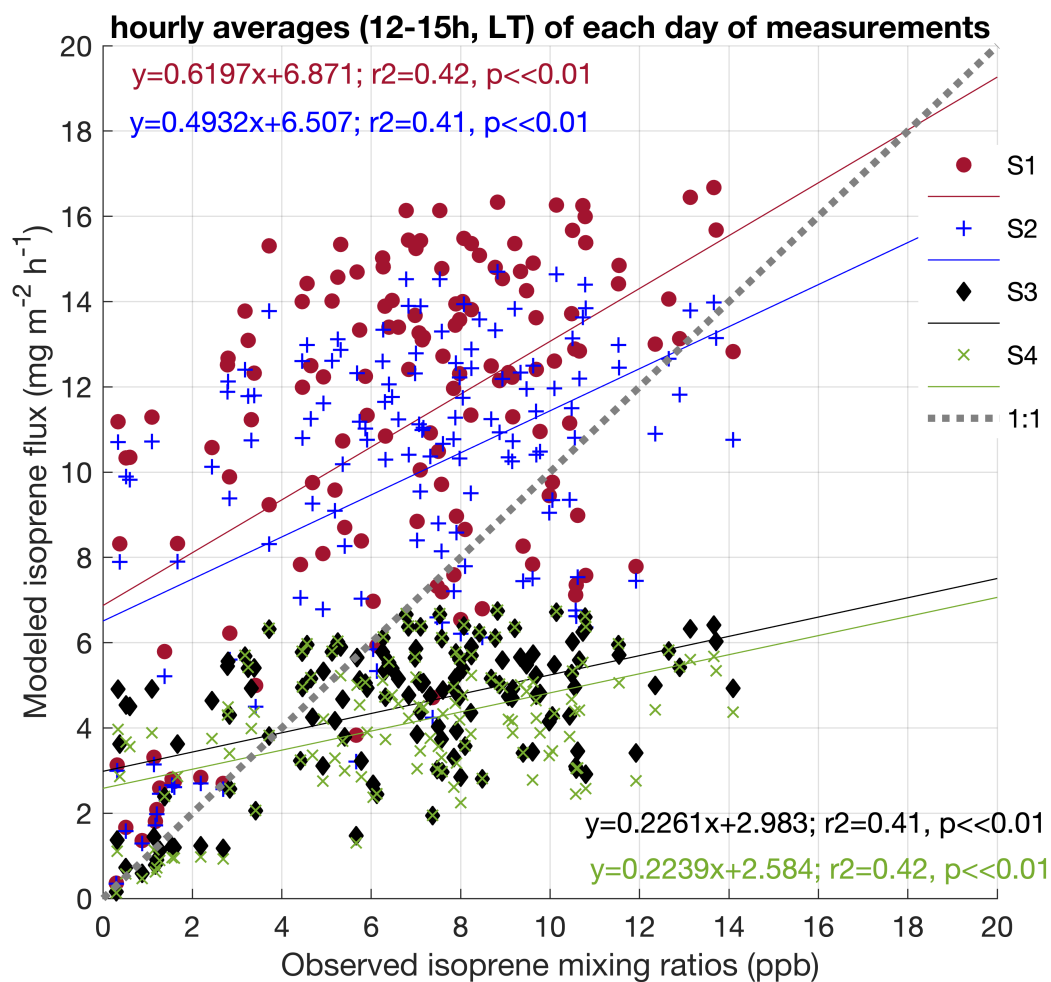
Figure 5. Simulated isoprene emission flux for 2014 and 2015. Monthly average of PPFD and air temperature (a, b) measured at the INSTANT tower. Simulations for 2014 (c) and 2015 (d) are: MEGAN simulation default, no change in the LAI code, emission factor equals to $7 \text{ mg m}^{-2} \text{ h}^{-1}$ and leaf age activity factor unmodified - S1; MEGAN simulation with change for LAI - leaf age classes, emission factor equals to $7 \text{ mg m}^{-2} \text{ h}^{-1}$ and leaf age activity factor unmodified - S2; MEGAN simulation with change for LAI - leaf age classes, emission factor equals to $3.21 \text{ mg m}^{-2} \text{ h}^{-1}$ and leaf age activity factor unmodified - S3; MEGAN simulation with change for LAI - leaf age classes, emission factor equals to $3.21 \text{ mg m}^{-2} \text{ h}^{-1}$ and leaf age activity factor modified - S4. Solid lines are means, and shaded areas represent one standard deviation of the mean.



1409
 1410 **Figure 6.** Observation of isoprene flux (eddy covariance) and MEGAN simulation for 11
 1411 days in November 2015. Half-hourly averages of PPFD and air temperature (a); EC
 1412 isoprene flux and MEGAN simulations (b); linear regression between EC isoprene flux and
 1413 PPFD (c); quadratic regression between EC isoprene flux and air temperature (d); linear
 1414 regression between simulations and PPFD (e); linear regression between simulations and
 1415 air temperature (f); linear regression between EC isoprene flux and simulations (g); daily
 1416 mean ratios between simulations and observation (h).

1417
 1418
 1419
 1420
 1421
 1422
 1423
 1424
 1425
 1426
 1427
 1428
 1429
 1430
 1431
 1432
 1433
 1434

1435



1436

1437

Figure 7. Correlation between isoprene mixing ratios observed at 38m during Feb and Mar 2014, Aug 2014, and Oct 2015, and the four simulations done for the respective periods.

1438

Data represent hourly averages (12-15h, local time (LT)) of each day of measurements (a).

1439

1440

1441

1442

1443

1444

1445

1446

1447

1448

1449

1450

1451